MARSH SEDIMENT ACCUMULATION AND ACCRETION ON A RAPIDLY RETREATING ESTUARINE COAST

by

Conor McDowell

A thesis submitted to the Faculty of the University of Delaware in partial fulfillment of the requirements for the degree of Master of Science in Marine Studies

Winter 2017

MARSH SEDIMENT ACCUMULATION AND ACCRETION ON A RAPIDLY RETREATING ESTUARINE COAST

by

Conor McDowell

Approved: _____
Christopher K. Sommerfield, Ph.D.
Professor in charge of thesis on behalf of the Advisory Committee

Approved: _____
Mark A. Moline, Ph.D.
Director of the School of Marine Science and Policy

Approved: _____
Mohsen Badiey, Ph.D.
Acting Dean of the College of Earth, Ocean, and Environment

Approved: _____
Ann L. Ardis, Ph.D.
Senior Vice Provost for Graduate and Professional Education

ACKNOWLEDGMENTS

This research was funded by National Fish and Wildlife Foundation grant #43752 to Dr. J.T. Kirby, University of Delaware. Additional support to the author was provided by the Marian R. Okie Fellowship and the University of Delaware.

The author would like to thank his advisor, Dr. Christopher Sommerfield, for all of his support and mentorship. He would also like to thank his committee members Dr. James Pizzuto and Dr. James Kirby for their guidance and input.

Kaitlin Tucker, Katherine Pijanowski, Brandon Boyd, and Daniel Duval, were essential in both the lab and the field.

Collaborators at the USFWS made this research possible. The author would like to thank Susan Guiteras, Laura Mitchell, Rodrick Murray, Collin Brown, and Curtis George at Bombay Hook NWR for their support.

TABLE OF CONTENTS

LIST OF TABLES

LIST OF FIGURES

ABSTRACT

Bombay Hook National Wildlife Refuge in coastal Delaware protects one of the most expansive salt marsh systems on the U.S. Mid-Atlantic seaboard. In recent decades, the Refuge has experienced a substantial decrease in salt marsh area along the Delaware Bay boundary by shoreface erosion and in the marsh interior by inland pool expansion. Although the origin of the pools is unknown, it has been suggested that the supply of allochthonous mineral sediment from tidal waterways to the marsh platform may be a contributing factor. To investigate whether vertical accretion of Refuge marshland is limited by sediment accumulation, a study was conducted to measure rates of mineral sediment and organic matter accumulation (mass/area/time) and accretion (length/time) using ^{137}Cs and ^{210}Pb chronologies developed for 19 marsh sites throughout the Refuge. To establish patterns and rates of recent historical marsh loss, an analysis of historical aerial photographs was undertaken.

Results indicate that Bombay Hook NWR has lost a total of ~8.6 million m^2 of marsh area since 1961. This loss was mostly caused by the formation of inland pools (~50% of area lost) and shoreface erosion along the Delaware Bay boundary (~35%), with a smaller contribution by waterway channel widening (~15%). Shoreface erosion was most prevalent in the southern half of the Refuge with some locations experiencing up to ~12 m/yr of retreat since 1961, while the northern section experienced far less retreat at 0.6 m/yr. The formation and expansion of inland pools were mostly concentrated in the northern half of the Refuge, adjacent to three freshwater impoundments constructed by the United States Fish and Wildlife Service in the late 1930s.

Salt marsh accretion and mass accumulation rates measured for this study fall within the middle to upper range of similarly determined rates for undisturbed marshes of the Delaware Estuary, and rates based on ^{137}Cs and ^{210}Pb methods were largely in agreement. Accretion rates (^{137}Cs) for low marsh sites averaged 0.65 cm/yr and were significantly higher than rates at high marsh sites, which averaged 0.42 cm/yr. Combined mineral and organic mass accumulation rates (^{137}Cs) exhibited a similar difference between low and high marsh sites, averaging 0.31 g/cm^2/yr and 0.13 g/cm^2/yr, respectively. Mineral and organic mass accumulation rates correlated strongly with rates of accretion (R^2= .85 and .79 respectively), revealing that both mineral sediment and organic matter drive marsh accretion at the Refuge, and that belowground biomass accumulation and aboveground mineral sediment deposition set the minimum and maximum rates of accretion, respectively.

Marsh accretion rates measured in this study met or exceeded the rate of recent relative sea-level rise for the middle Delaware Estuary, based on the NOAA tide gauge record for Reedy Point (0.35 ± 0.05 mm/yr, 1956-2015). This result, in combination with the high rates of mineral accumulation measured throughout the Refuge, makes clear that there is not a marsh accretionary deficit related to insufficient mineral sediment. Moreover, the marsh soil record provides no evidence that the formation and expansion of marsh pools since the 1960s is related to low rates of marsh accretion or sediment supply. Additional research on historical changes in tidal inundation, marsh accretion, and elevation change is needed to better understand the nature of pool expansion and marsh loss at the Refuge.

Chapter 1

INTRODUCTION

Tidal wetlands of estuaries and deltas worldwide are threatened by a wide range of natural and anthropogenic influences ranging from accelerated sea level rise to changes in coastal land use (Coleman et al., 2008; Kirwan and Megonigal, 2013). Tidal wetlands provide important habitat for juvenile fish and seabirds, sequester atmospheric carbon dioxide, and protect coastal infrastructure from storms, thus loss of these ecosystem services has significant environmental and economic implications. Some projections on the survivability of tidal wetlands are bleak (Nicholls et al, 1999). For example, in the case of mid-latitude salt marshes, historical rates of wetland loss suggest near complete marsh loss in regions like the Chesapeake Bay (Reed et al., 2008). On the other hand, some authors paint a more optimistic picture, suggesting that ecosystem-scale feedback mechanisms have potential to provide sufficient defense against accelerated sea-level rise provided there is sufficient sediment availability for marsh accretion (Stralberg et al.,2011; Schuerch et al., 2013; Kirwan et al., 2016).

Salt marshes can be divided into two types, estuarine and coastal, based on their geomorphic setting and soil properties (Darmody and Foss, 1979). Estuarine marsh soils are often very minerogenic, by reason of their proximity to fluvial sediment input, erosion within the estuary and marine sources. Consequently, estuarine marshes exhibit higher rates of sediment accumulation and accretion than coastal marshes (Boyd et al., 2017) and may be less prone to inundation by accelerating relative sea-level rise.

Since the last glaciation much of the U.S. Atlantic Coast has been undergoing marine transgression caused by global sea level rise and regional land subsidence. In estuaries, transgression is characterized by landward and upward migration of the shoreline in advance of an eroding shoreface (Dalrymple et al., 1992). As the estuary widens and the tidal prism increases, the head of tides and saltwater intrusion migrate progressively landward. Shoreface erosion by wind-waves and tidal currents destroys tidal wetlands along transgressive coasts, whereas new wetlands are gained by landward migration of wetland plants into higher-elevation lowlands. Although wetland loss is a natural outcome of the lifecycle of estuaries and deltas (e.g., Wells and Coleman, 1987), the processes and patterns of loss are complex and difficult to predict. Superimposed on natural processes of wetland loss are anthropogenic factors including conversion of marshland to upland and hydrologic alteration (Gedan et al., 2009). This superposition of natural and human-driven change greatly complicates wetland management and restoration strategies.

In this study, Bombay Hook National Wildlife Refuge (NWR) is presented as a case study of a human-altered tidal wetland complex on a rapidly transgressing estuarine coast. The Refuge is located on the western shore of the Delaware Estuary at the transition between wave-dominated sandy shorelines to the south and mud-dominated wetland shorelines to the north (Fletcher et al., 1992). Since the late 19th Century, the shoreline at the open boundary of the Refuge has been retreating at a mean rate of ~2 m/yr, and within the Delaware Estuary is a hotspot of shoreface erosion (Pijanowski, 2016). Additionally, marsh pond expansion during the past ~75 years has significantly decreased the area of vegetated marsh. Refuge managers and the State of Delaware are concerned about the rapid loss of the salt marsh platform and in recent

years have taken measures to better understand the underlying processes. The observational study described in this thesis 1) quantified lost marsh area over the past 55 years, and 2) measured marsh accretion and sediment accumulation rates to provide context for ongoing Refuge management and research efforts.

Chapter 2

BACKGROUND

2.1 Marsh Accretion and Elevation Change

Conceptual models of salt marsh development have been proposed by numerous researchers and adapted into predictive models that assess marsh vulnerability to changes in tidal hydrology and sedimentation conditions (e.g., French, 2006). The stability of the marsh platform depends on its elevation within the tide frame. To maintain an elevation between mean tide level and mean high water, the zone of maximum belowground biomass production (Morris et al., 2002), the elevation of the marsh platform must rise, or accrete, at a rate greater than or equal to the rate of relative sea level (RSL) rise. This equilibrium is maintained by the accumulation of mineral sediment and organic matter (Redfield, 1972; Allen, 2000); the former is transported in suspension to the marsh platform, while the latter is deposited as organic detritus or produced in situ as roots, rhizomes, stems, and leaves. Sediment accumulation is offset by subsidence, including autocompaction of surface sediment layers and deeper isostatic adjustment, which lowers the elevation of the marsh platform. A simplified view of this relationship was described by French (2006) and is given by:

$$\Delta E = \Delta S_{min} + \Delta S_{org} - \Delta C - \Delta M \quad (1)$$

where elevation change (ΔE) of the marsh relative to RSL in a period of time equals the amount of vertical sediment accretion ($\Delta S_{min} + \Delta S_{org}$), minus sediment compaction (ΔC), minus the rise in RSL (ΔM) over the same time period.

Interactions among local hydrodynamics, sediment supply, elevation, and ecologic processes control soil volume which drives vertical accretion of the marsh platform (Figure 1). Pethick (1981) proposed that rates of sediment accumulation and

accretion are influenced by the depth and frequency of flooding. Because lower elevation areas are flooded more frequently and for longer durations, suspended particles have more time to settle. As elevation within the tidal frame increases, the rate of accretion decreases, eventually reaching an equilibrium value at or near the rate of RSL rise. This relationship has been observed in some marshes over short time scales (French and Spencer, 1993; Cahoon and Reed, 1995), but not all marshes exhibit this pattern (van Proosdij et al., 2006; Boyd et al., 2017).

Elevation and tidal hydroperiod also play a role in determining the volume and structure of organic matter present in marsh soil. For every species of plant on the marsh platform there is an optimal elevation where primary production and biomass formation are maximal (Morris et al., 2002). When the marsh elevation falls above this optimal elevation, marsh flooding occurs infrequently and evapotranspiration increases soil salinity to levels lethal to plants. When the elevation is too low, sulfide accumulation and hypoxia in the soil decrease productivity, biomass formation, and soil volume. When excessive these processes may result in marsh dieback and cause the marsh to revert to a pan or unvegetated mudflat.

2.2 Processes that Control Marsh Boundaries

Observations and numerical modelling of salt marshes have shown that the seaward marsh boundary is unstable, retreating landward and extending seaward under variation conditions of wind waves and sediment supply (van der Wal et al., 2008; Mariotti and Fagherazzi, 2010). Areas that are regularly flooded and maintain an elevation that approaches mean high water will remain marshland. As RSL rises, an established marsh will increase its surface elevation by accreting at approximately an equal rate to maintain the optimal position within the tide frame (Morris et al., 2002).

Saltwater intrudes into upland areas, killing freshwater plants and allowing for the upland migration of marsh vegetation—this influences the landward boundary of the marsh. As the marsh migrates landward, hydrodynamic and meteorological processes cause platform loss in other sections of the marsh. The most common of these processes is edge erosion by waves, the chief mechanism of marsh loss in coastal environments (Marani et al., 2011). Edge erosion often occurs at the shoreface where fetch and water depth allow for maximum wave power. The presence of wetland plants in the intertidal zone has been suggested to reduce rates of wave erosion (Möller et al., 2014), however, other studies have refuted this claim (Feagin et al., 2009).

Another mechanism of marsh deterioration is the formation of inland pools, which are unvegetated depressions filled with salt water throughout the tidal cycle (reviewed by Mariotti, 2016). These pools form when marsh vegetation dies, either through physical processes, such as ice rafting or wrack deposition, or biogeochemical processes related to root waterlogging or high soil salinity (Van Huissteden and Van de Plassche, 1998). When waterlogging occurs, anaerobic decomposition of organic matter and sulfate reduction may destroy soil structure created by living roots and rhizomes, causing local subsidence and increasing pool depth. This has been observed by DeLaune et al. (1994) who attribute ponding to peat porosity collapse. Studies have noted that the area of pools in salt marshes worldwide has increased (Pethick, 1974; Kearney et al., 1988; Hartig et al., 2002), which some authors attribute to sea level rise and accretionary deficits. Alternatively, Wilson et al. (2014) suggest that the formation of pools may be related to the drainage characteristics of the salt marsh complex, independent of marsh platform accretion. Wilson et al. (2009, 2010) describe marsh pools as temporary, cyclic features that form, enlarge, and infill as plants revegetate. As

pools enlarge and deepen, they become more susceptible to erosion by locally derived wind waves, which in some cases may cause irreversible marsh erosion (Mariotti and Fagherazzi, 2013; Mariotti, 2016).

Chapter 3

STUDY AREA

3.1 Geologic Setting

Bombay Hook NWR protects one of the largest expanses of salt marsh in the Mid-Atlantic United States. The Refuge serves as an important habitat for migratory birds, and is recognized nationally as a top birdwatching location (United States Fish and Wildlife Service, 2014). As a result, the Refuge attracts out-of-state visitors who provide millions of dollars annually to the local economy (Kauffman et al., 2011). The Refuge fringes the confluence of the Leipsic River and the western shore of the Delaware Estuary, which formed in the incised valley of the ancestral Delaware River (Figure 2).

Tidal marsh wetlands, including salt, brackish, and freshwater marshes, have fringed the estuary since early Holocene times (9-7 ka). Following the collapse of the Laurentide Ice Sheet and ensuing deglaciation, thermosteric expansion of ocean water caused sea levels to rise globally. Coupled with rising global sea level was regional subsidence related to relaxation proglacial forebulge and compaction of coastal plain strata (Horton et al., 2013; Nikitina et al., 2015). Together, rising sea level and sinking land caused Delaware Estuary submerge and widen during the Holocene (Knebel et al., 1988). According to Nikitina et al. (2015), between 2200 and 150 yr BP the average rate of RSL rise in the Delaware Estuary region was 1.25 ± 0.27 mm/yr, mostly due to subsidence. Land elevation surveys by Holdahl and Morrison (1974) suggest that the Bombay Hook area is a hotspot of subsidence with rates on the order of 2-3 mm/yr. Rates of historical RSL rise from NOAA tide gauges at Reedy Point and Lewes, Delaware, are 3.54 ± 0.51 mm/yr (1956-2015) and 3.4 ± 0.24 mm/yr (1919-2015),

respectively. Hence, subsidence makes a significant contribution to RSL rise in the estuary.

Fletcher et al. (1992) describe a conceptual model relating the migration of the estuarine turbidity maximum and the transgressive evolution of the estuary. In this model, they propose that areas located adjacent to turbidity maximum are constructive because of ample sediment accumulation and creation of intertidal flats, which provides substrate for marsh growth, whereas areas to the south are destructive due to loss of the fine sediment supply. As the turbidity maximum migrated landward under the combined influences of land subsidence and rising sea level, areas of rapid sediment accumulation along the tidal wetland coast became increasingly exposed to wave energy within the widening estuary. Ultimately, this results in formation of a retreating barrier beach, composed of sand derived from eroding headlands. The barrier beach separates salt marsh from open estuary waters.

Nikitina et al. (2003) report that Bombay Hook began to experience transgression 5 ka with the formation of brackish marsh within the Leipsic River Valley. These brackish conditions continued until about 1 ka when salt marshes began to replace brackish marshes as the dominant facies. This timeline is consistent with the one described by Fletcher et al. (1992), which places the turbidity maximum depocenter at the confluence with the Leipsic River between 6 ka and 4 ka. Today, the turbidity maximum zone of the estuary extends from the mouth of Christina River seaward to Artificial Island, approximately 22 km north of the study area (Sommerfield and Wong, 2011). A recent study of shoreline change in the Delaware Estuary by Pijanowski (2016) identified the Bombay Hook area as a hotspot of erosion with shoreline retreat rates reaching 4 m/yr in places, averaged since the late 19th Century.

3.2 Wetland Vegetation and Hydrology

The dominant vegetation on the marsh platform is *S. alterniflora* and *S. patens* with isolated bands of the invasive *Phragmites australis* found along the estuary shore and Refuge waterways. Most of the salt marsh at the Refuge is low marsh *S. alterniflora* (55%), with high marsh *S. patens* and *Phragmites* comprising 35% and 10%, respectively, of the total area of marsh. A north-south band of higher-elevation marsh borders the Delaware Estuary and is mostly populated by *Phragmites* with intermixed *S. cynosuroides*. This high-elevation band of vegetation prevents regular tidal flooding from the estuary across the open boundary of the marsh (Figure 3). As for why *Phragmites* can thrive immediately adjacent to high salinity waters of Delaware Estuary, Phillips (1987) theorizes that overwashes of sand and wrack during storms promote *Phragmites* invasion by 1) killing low marsh *S. alterniflora*, and 2) increasing ground elevation just enough to limit tidal flooding and accumulation of sulfide in the soils.

Refuge marshes are divided into eight management units and fringe four wide and deep tidal waterways that connect to the Delaware Estuary (Figure 2). The four northernmost units are drained by two openings, Sluice Ditch to the north and the Leipsic River to the south. These two openings are connected by Duck Creek, a tidal channel that continues to the estuary shore north of the Refuge boundary. These northern waterways are the deepest in the Refuge and reach 15-m deep at their deepest points. The southernmost units are drained by the slightly shallower Simons and Mahon Rivers (~11 m at their deepest points), which are connected by a series of smaller tidal channels. Prior to the mid-19th Century, the Leipsic and Simons rivers converged at a single inlet to the east of the current shoreline. Since that time the shoreline has eroded landward of the confluence of these rivers to form two tidal inlets. Spring tide range in

Refuge waterways ranges from 2.0 to 2.5 m (DNREC unpublished data), somewhat larger than the tide range in adjacent estuary waters (1.9 m at Ship John Shoal).

3.3 Human Intervention

Human occupation of the Delaware coast has resulted in rapid changes to the marshes of Bombay Hook. During colonial times, channels and ditches were created to provide routes for inland transportation and to drain lands for agriculture. Although the exact dates of trenching are unknown, Sluice Ditch at the northern end of the Refuge and Raymond Gut, which runs south into the Leipsic River, are examples of this colonial dredging. Since its inception as a National Wildlife Refuge in 1937, further human intervention followed. As in many U.S. Atlantic coast marshes, the Civilian Conservation Corps grid-ditched the southern end of the Refuge for mosquito control in the 1930s. These ditches were maintained by the State of Delaware through the late 1960s (DELDOT, 1963). To promote birdwatching, Shearness, Raymond, and Bear Swamp Pools, three large freshwater impoundments (~1.5 km, ~0.5 km, and ~1.25 km diameter respectively), were constructed north of the Leipsic River as waterfowl habitat (Figure 2). Water levels in these pools are controlled by one-way tide gates that connect to the adjacent Money Marsh.

Money Marsh is a particular area of concern for Refuge managers because of the growth of wide (~1 km), shallow (~1.5 m) pools on the low marsh platform in recent decades (Figure 2). Aerial photography and topographic quadrangles from the 20th Century suggest that the initialization of these pools began before 1937 in the northwest corner of their present location. The rate of pool expansion appears to have accelerated between 1968 and 1992, after which expansion seems to have ceased. The cause and timing of pool formation at the Refuge is unknown.

Previous studies of marsh loss at Bombay Hook NWR have focused on denudation of the marsh platform near Money Marsh due to grazing by migrating Canada and snow geese. Wetlands Research Associates, Inc. (1995) described geese "eatouts" that repeatedly occur in the Money Marsh section of Bombay Hook and have been reported since the 1930's. Young (1985) calculated a loss of 539 acres of salt marsh between 1980 and 1984. Her study concluded that "eatouts" cause delayed maturation of and a reduction in plant height, however, no change was found in belowground growth. In the year following "eatouts", ungrazed plants have been able to restore the marsh platform demonstrating an ability to rapidly recover. Monitoring of geese populations in at the Refuge between 1976 and 1993 indicated an increasing trend of snow goose foraging at the Refuge. However, a comparison of *Spartina alterniflora* cover over the same time period indicated that the marsh appears to be able to recover (Smith, 1994).

The purpose of the present study was to investigate salt marsh sedimentation conditions at the Refuge to provide context for ongoing studies of marsh loss by inland pooling and estuary shoreface erosion. Following observations of marsh loss by pooling in other tidal wetland systems (e.g., Day et al., 2011), it was hypothesized that pooling after ~1950 is a consequence of a marsh accretionary deficit caused by insufficient mineral sediment supply from adjacent tidal waterways. To test this hypothesis, marsh accretion and sediment accumulation rates were measured by ^{137}Cs and ^{210}Pb chronometry at 19 sites throughout the Refuge and compared to local tide-gauge records of RSL rise. Additionally, patterns and rates of marsh loss were quantified through an analysis of historical aerial photographs. The findings from this study will

be used to guide the management and restoration decisions of refuge managers moving forward.

Chapter 4

METHODS

4.1 Analysis of Marsh Topography

To investigate changes in the spatial extent of salt marsh (in exclusion of tidal flats and waterways) at the Refuge, marsh boundaries traced from 1961 and 2012 aerial photography were manually digitized and compared in a GIS. The earliest photographs were taken during a series of flights between 1960 and 1961 by the Agricultural Stabilization and Conservation Service. These photographs were scanned and georectified by the Delaware Geologic Survey using a 2002 dataset as a guide (Delaware Geologic Survey, 2006a). Obvious warping of images occurred north of Money Marsh (Figure 2), so imagery from 1968 was used in that section instead (Delaware Geologic Survey, 2006b). The second set of aerial photographs was extracted from 2012 orthoimagery available from the United States Geological Survey (United States Geological Survey, 2012). These 0.3-m resolution photographs have a horizontal error of 1.52 m. A conservative horizontal error estimate of 5 m was used for the edge of the 2012 marsh platform (1.52 m horizontal error + 0.5 m digitizing error + 3 m edge identification error), and 10 m was used for the 1961/1968 platform (5 m photo distortion error + 2 m georeferencing error + 1 m digitizing error + 3 m edge identification error). The digitized boundaries were then overlaid to identify locations of marsh gain and marsh loss during the intervening period.

A hypsometric analysis of marsh elevation was conducted to describe the flooding regime on the marsh platform. A combined bathymetric and topographic grid developed by Abdolali et al. (2016) based on 2011 LiDAR data collected by the Delaware Department of Natural Resources and Environmental Control (DNREC)

(DNREC, 2012) was used to develop hypsometric curves representing the percentage of area above a given elevation for the entire marsh complex (Figure 4). Additionally, curves for the northern and southern sections of the Refuge (above and below the centerline of the Leipsic River) were constructed. Mean low water, mean high water, and mean tide level reference elevations were determined from achieved water level data obtained by four sensors maintained by DNREC since 2010 (DNREC, unpublished data).

4.2 Core Collection

Nineteen coring locations were selected in an effort to characterize the full range of marsh elevations and plant communities at the Refuge. The cores were collected during the summers of 2015 and 2016 (see Table 2 and Figure 3 for locations). Where possible, coring sites were selected near (within 20 m) of previously installed Surface Elevation Tables, which have known elevations relative to NAVD88. If a Surface Elevation Table was not located near a coring location, a corrected 1-meter LiDAR grid (DNREC, 2012) was used to approximate elevation (vertical error ± 10 cm) (Abdolali et al., 2016). A 4-inch diameter, sharp-edged PVC coring tube was cut into ~1-m lengths, and cores were collected by pushing the tube into the marsh surface using a piston-tripod-winch device to reduce core shortening upon insertion and slipping on extraction. Core were collected at 100% recovery (no shortening) by this method. Once collected, cores were sealed, brought to the lab, and stored at 4˚C until processed. In the lab, cores were extruded vertically and sub-sampled into 2-cm thick sections for radionuclide and physical property analyses.

4.3 Physical Property Measurements

For each 2-cm interval, soil water content, dry bulk density, bulk mineral density, bulk organic density, porosity, and radionuclide activity concentrations were measured. Each interval was dried for 24h at 105˚C to determine water content (W) gravimetrically as described in the equation below:

$$W = \frac{WW - DW_{105}}{WW} \tag{2}$$

where WW is wet weight and DW_{105} is dry weight.

The relative contribution of organic and mineral sediment was determined via loss-on-ignition following the method described by Heiri et al. (2001). After combustion the residual ash was considered to represent the fraction of mineral sediment in the sample. Following the method of Federer et al. (1993), this allowed for the calculation of dry bulk density (ρ_d) as:

$$\rho_d = \frac{1-W}{\frac{W}{\rho} + \frac{1-W}{\rho_s}} \tag{3}$$

where ρ is the average density of pore fluid (1.02 g/cm^3) and ρ_s is the bulk density of the solid fraction calculated as ((1 – LOI) x 2.65) + (LOI x 1.2), where 2.65 and 1.2 are representative densities (g/cm^3) for mineral and organic solids, respectively. Hence, the respective concentrations (g/cm^3) of the organic matter (C_{org}) and mineral sediment (C_{min}) in the soil are given by:

$$C_{min} = (1 - LOI) * 2.65 \tag{4}$$

$$C_{org} = LOI * 1.2 \tag{5}$$

Based on sample triplicates, the LOI measurements had an uncertainty of ±2%. From the bulk density measurements, the relative volume (in percent) of the soil contributed by pore space, mineral solids, and organic solids was calculated for each core interval. Note that the method described above does distinguish between porosity associated

with interstitial voids between solids and the porosity of living and dead plant tissue, such as roots and rhizomes.

4.4 Radionuclide Geochronology

A total of 510 core subsamples were prepared for gamma spectrometry following methods similar to those described by Wallbrink et al. (2002). Dry samples were uniformly milled and packed into 60-ml plastic screw-lid jars at a uniform density using a hydraulic press. Samples were then counted for 24-48 hours on either a Canberra Model GL2020R low energy germanium detector with ultra-low background components, or a Canberra Model 2825 broad energy germanium detector with ultra-low background cryostats. A spectroscopic analysis of photopeaks was used to determine the activities for the radionuclides ^{210}Pb, ^{214}Bi, and ^{137}Cs. In this analysis the minimum detectable activity was ~3 MBq/g. Unsupported, excess ^{210}Pb activity ($^{210}Pb_{xs}$) was determined from measurements of total activity using ^{214}Bi as a proxy for minerogenic ^{226}Ra, the source of supported ^{210}Pb activity in the soils ($^{210}Pb_{xs} = {}^{210}Pb_{total} - {}^{214}Bi$). Propagated one-sigma detector background, detector calibration, and sample counting errors are reported with the data.

Inventories of ^{137}Cs and $^{210}Pb_{xs}$ in the soils were calculated to determine spatial variation in radionuclide supply to the marsh platform by direct atmospheric deposition and indirect tidal deposition of particulates. Radionuclide inventories were calculated as follows:

$$I = \sum_{i=1} \rho_{di}\, x_i A_i \qquad (6)$$

where, I is the radionuclide inventory (mBq/cm^2), ρ_d is the dry bulk density for the interval (g/cm^2), x is the thickness of the interval (2 cm), A is the specific activity

(mBq/g) and i indicates the interval number downcore. Inventories were considered "complete" if activities of ^{137}Cs and $^{210}Pb_{xs}$ were not present at the bottom of the core.

4.5 Accretion and Accumulation Rates

Rates of marsh accretion (length/time) and mass accumulation rates (mass/area/time) were computed from ^{137}Cs activity profiles using the activity peak as an indicator of the year of maximum fallout in 1963 (e.g., Nyman et al., 2006). The depth of the peak divided by years elapsed between 1963 and the year of core collection provides the accretion rate. Error bars for the ^{137}Cs-derived accretion rates were calculated by considering 1 cm of vertical error in the depth of the peak. In cases where the uncertainty in ^{137}Cs activities caused an ill-defined peak, both intervals were considered in depth calculation errors. Downward "tailing" of ^{137}Cs was observed in some cores, so the first occurrence of ^{137}Cs in the profile, consistent with the environmental onset of ^{137}Cs in 1954, was not used as a chronological marker (DeLaune et al., 1978). Rates of marsh accretion and accumulation were also measured using ^{210}Pb in an attempt to develop a longer (~100 year) chronology. Whereas the ^{137}Cs peak provides an absolute date, ^{210}Pb is a relative dating method with a variable dating range dependent on the initial surface activity.

The relationship between $^{210}Pb_{xs}$ activity and accretion rate at steady state is given by:

$$AR = -\lambda \cdot \frac{z}{ln(A_o/A_z)} \tag{7}$$

where λ is the decay constant for ^{210}Pb (0.0311 y^{-1}), AR represents the accretion rate (cm/yr), A_0 is the initial activity of $^{210}Pb_{xs}$ (mBq/g) at the surface of the core, and A_z is the activity of $^{210}Pb_{xs}$ (mBq/g) at depth z (cm). This equation represents the Constant

Flux-Constant Sedimentation (CFCS) ^{210}Pb model, which assumes that both sedimentation rate and flux of $^{210}Pb_{xs}$ remain constant down-core (Robbins, 1978; Appleby and Oldfield, 1992). The CFCS model uses the slope of the least-squares linear regression of the full profile of the natural log of $^{210}Pb_{xs}$ activity plotted against depth, not the activities of individual intervals as other ^{210}Pb models like the Constant Initial Concentration model, to determine the accretion rate (cm/yr). Error bars for accretion rates determined using Eq. 7 were calculated using the 95% confidence interval for the least squares regression.

Mass accumulation rates (MAR, g/cm^2/yr) were similarly calculated following Eq. 7 by plotting the natural log of $^{210}Pb_{xs}$ activity against cumulative mass (CM, g/cm^2), the product of the sample interval thickness (cm) and soil dry bulk density (g/cm^3) integrated over the sampling depth. Mass accumulation rates account for down-core variations in soil bulk density and normalize ^{210}Pb activity concentrations expressed in mass units (mBq/g). The age of a soil layer (t) is related to CM and MAR as follows:

$$t = \frac{CM}{MAR} \tag{8}$$

Confidence intervals reported with ^{210}Pb-derived accretion and mass accumulation rates were computed from the 95% confidence envelope of the least-squares linear regression.

Chapter 5

RESULTS

5.1 Marsh Topography and Spatial Distribution

The analysis of LiDAR topography indicated that about 40% of the salt marsh falls above mean high water (MHW), 40% between MHW and mean tide level (MTL), 5% between mean MTL and MLW, and 15% below MLW (Figure 5). The hypsometric curve implies that about 80% of the marsh complex is marsh platform, whereas the area between MTL and MLW consists of intertidal flats. Comparison of hypsometry for the northern and southern sections of the Refuge reveals that the northern marsh is ~10% mudflat area, while only 5% of the southern section is mudflat. This difference is explained by the presence of the pooled Money Marsh in the north. Both the northern and southern sections of the marsh are both composed of approximately 15% open waterway (tidal channel) area.

Based on the analysis of aerial photographs, in 1961 the area of salt marsh at the Refuge was 47,936,000 ± 2,714,000 m^2. By 2012 the Refuge had lost ~20% of that marsh platform for a net loss of 169,000 ± 9,000 m^2/yr (Table 2). The spatial pattern of loss is shown in Figure 6. As expected, the regions of most rapid loss are the shoreface along Delaware Estuary and within the marsh interior in the northern section of the Refuge where large pools formed—the highest rates of marsh loss occurred either in areas of high energy (shoreface) or low elevation (pools).

To further characterize patterns of marsh extent at the Refuge, locations of marsh loss or gain were classified according to their proximity to the waterways (Figure 6, Panel 4). Areas of loss or gain adjacent to the estuary shoreface were classified as *shoreline change*, whereas changes along tidal creeks were classified as

tidal creek widening or migration. *Inland pooling* was classified as expansions in non-channelized areas, which could either be attached or unattached to tidal creeks. Landward extension or loss of salt marsh along the western boundary of the Refuge was classified as *upland change*.

Of the 8.6 million m^2 of lost marsh, approximately half was due to inland pooling (Table 2). These pools were mostly concentrated in the northern half of the Refuge, adjacent to the impoundments (Bear Swamp Pool, Shearness Pool, and Raymond Pool). Approximately 35% of the marsh lost during this time period was due to shoreface erosion and landward retreat of the shoreline. Erosion was most intense in the southern part of the Refuge with some locations experiencing ~12 m/yr since 1961. During this time period, the northern section of shoreline experienced far less erosion (~0.6 m/yr). Tidal creek widening or migration comprised the balance (~20%) of marsh loss, which was evenly distributed across the tidal wetland complex. Recorded upland changes were minimal in this study. In the northern section of the Refuge, the freshwater impoundments prevented any possible marsh migration. Along the Leipsic and Simons Rivers, upland areas were inland, and therefore not captured in this study.

5.2 Marsh Soil Physical Properties

Dry bulk density in the salt marsh soils ranged from 0.08 g/cm^3 to 0.62 g/cm^3 with the highest values found along Sluice Ditch on the northern end of the study area (Table 1, Figure 7). In general, bulk density was uniform with depth in cores, and in only three of the cores (discussed below) were there noteworthy down-core changes. Previous studies have shown that bulk density increases with depth because of compaction (Ward et al., 1998; Bricker-Urso et al., 1989, Kearney et al., 1994), but this was not observed for soil profiles measured for this study. Overall, organic matter

concentration (Eq. 5) was uniform with depth at ~0.1 g/cm^3 with a slight increase in the top 5-10 cm. Since the organic matter concentration was more-or-less consistent among the sampling sites, differences in the total dry bulk density were mostly related to differences in mineral sediment concentration (see Eq. 4).

Results of a Welsh's t-test indicated that the mean bulk density of low marsh soils (mean bulk density = 0.44 g/cm^3, $\sigma = 0.08$) was significantly higher than that of the high marsh soils (mean bulk density = 0.29 g/cm^3, $\sigma = 0.06$). Two exceptions were soils at sites characterized by mixed high-marsh (STEAM03) and low-marsh (KENT01) vegetation which had relatively high and low bulk densities, respectively (Figure 7). Cores LTHB01, INT2, and AFA02A displayed marked down-core decreases in bulk density. For example, at a depth of 33 cm in core LTHB01, there was a decrease in bulk density from ~1.5 g/cm^3 to ~0.4 g/cm^3 mostly due to an increase in mineral sediment concentration. Similarly, soil profiles for sites AFA02A and INT2 display a down-core decrease in bulk density, again, due to a decrease in mineral sediment concentration from top to bottom. Since these decreases were not observed at the other coring sites, it evokes localized changes in the supply or trapping efficiency of allochthonous mineral sediment.

Another way of presenting the marsh soil properties is in terms of soil volume composition (Figure 8). Volume composition may be more meaningful than mass concentration because it conveys the relative contributions of organic matter, mineral sediment, and pore space on soil volume and marsh accretion rate. Overall, soil volume at the coring sites is composed of mostly water (73 – 96%) with lesser contributes by mineral (2 – 20%) and organic (2 – 12%) solids.

5.3 Radionuclide Activity Profiles and Inventories

Radionuclide inventories and accretion rates are listed in Table 3, and core profiles are presented in Figures 9, 10, and 11. Complete ^{137}Cs inventories were present in 12 of the 19 cores and ranged from 88.4 ± 6.d mBq/cm^2 to 235.8 ± 20.6 mBq/cm^2. These results fall within the range of reference inventories established for Mid-Atlantic region soils by Graustein and Turekian (1986) (82-250 mBq/cm^2); however, some of the higher inventories at the Refuge fall near the upper end of the reference range, perhaps due to a non-atmospheric source of ^{137}Cs. In all but three of the cores ^{137}Cs activity was detected at the surface, which, given that atmospheric fallout of ^{137}Cs has been negligible since the 1980s, suggests that there is a reworking of previously deposited ^{137}Cs. A ^{137}Cs peak was detected in 17 of the 19 cores (Figure 9). The depth of the peak ranged from 9 cm at STEAM03 to 49 cm at SD2. INT1 and SD1, the two cores lacking a ^{137}Cs peak, were both longer than 50 cm. These cores showed an upward trend in ^{137}Cs activity from the bottom of the core, suggesting that the activity peak fell below the maximum depth of coring.

In all cases profiles of total ^{210}Pb activity were characterized by exponential decay to supported levels (Figures 10 and 11). The maximum depth of $^{210}Pb_{xs}$ activity generally fell 15-20 cm deeper than the ^{137}Cs activity peak and covered a timespan on the order of 80-100 years. In GI01 and INT3, high marsh cores along Duck Creek, there was some deviance from the idealized steady-state decay profile between 10 and 25 cm depth. Excess ^{210}Pb inventories ranged from 438.69 ± 28.94 mBq/cm^2 to 1768.65 ± 164.08 mBq/cm^2. The upper end of this range exceeded atmospherically-sourced values previously reported for this region (Graustein and Turekian, 1986) (327-523 mBq/cm^2). Because the ^{137}Cs and $^{210}Pb_{xs}$ equaled or exceeded the regional reference inventories, it

is assumed that the soil chronostratigraphy is complete and not outwardly influenced by non-deposition or erosion.

5.4 Marsh Accretion and Accumulation Rates

Cesium-137 and $^{210}Pb_{xs}$ accretion rates for the cores in this study are listed in Table 3 and displayed graphically in Figure 12. The depths of the ^{137}Cs activity peaks ranged from 9 to 45 cm, equating to accretion rates between 0.17 ± 0.10 and 0.92 ± 0.02 cm/yr with an overall mean of 0.5 ± 0.13 cm/yr. In all cases the ^{137}Cs peaks were distinct suggesting that they had not been subjected to significant biological mixing. Accretion rates for each core were also calculated using profiles of $^{210}Pb_{ex}$ following Equation 7. These rates ranged from 0.29 ± 0.2 to 1.33 ± 0.06 cm/yr. Although there can be methodological differences in measured accretion rates, a Welsh's t-test found no difference between the means of the ^{137}Cs and ^{210}Pb rates determined for this study (p-value = .56, n = 17).

Results of a Welsh's t-test indicated that the average ^{137}Cs-derived accretion rate at low marsh sites (mean accretion rate = 0.65 cm/yr, $\sigma = 0.21$) was significantly higher than those at high marsh sites (mean accretion rate = 0.43 cm/yr, $\sigma = 0.09$). These average rates are similar to those reported in a meta-analysis of North American and European salt marsh accretion rates by Kirwan et al. (2016). In general, lower accretion rates at high marsh sites has been interpreted to reflect less frequent tidal flooding that low marsh sites and less mineral sediment deposition (Redfield, 1972). This interpretation is consistent with results of the present study, which indicate higher concentrations of mineral sediment in the low marsh soils.

Cesium-137 derived rates of mineral sediment and organic matter accumulation calculated using Equation 8 are listed in Table 3 and presented in Figures 13 and 14. A

Welsh's t-test indicated that the average ^{137}Cs-derived total mass accumulation rate at low marsh sites (mean mass accumulation rate = 0.31 g/cm^2/yr, σ = 0.13) was significantly higher than those at high marsh sites (mean mass accumulation rate = 0.13 g/cm^2/yr, σ = 0.05). Mineral and organic mass accumulation rates correlated strongly with rates of accretion (R^2= .85 and .79 respectively) (Figure 15). These strong correlations imply that both mineral sediment and organic matter contribute to accretion of Refuge marshes, and that belowground biomass accumulation and above ground mineral sediment deposition set the minimum and maximum rates of marsh accretion, respectively.

Previous studies have demonstrated that marsh accretion and accumulation rates have an inverse relationship to elevation on a transect scale as increased flooding frequency and duration allows for more sediment to be deposited on the marsh platform (Pethick, 1981; French, 1993). In this study, regression analysis indicated no apparent relationship between marsh surface elevation and measured accretion or mass accumulation rates, consistent with prior studies of marsh accretion in the Mid-Atlantic region (Boyd et al., 2017).

Chapter 6

DISCUSSION

6.1 Marsh Accretion Rates and Relative Sea-level Rise

Salt marsh accretion rates calculated for this study fall within the middle to upper range of similarly determined rates for undisturbed marshes of the Delaware Estuary (Kraft et al., 1992, Kim et al., 1997; Kim et al., 2004; Boyd and Sommerfield, 2016; Boyd et al., 2017) and elsewhere in the Mid-Atlantic region (Armento and Woodwell, 1975; Bricker-Urso et al., 1989; Carey, 1996; Anisfeld et al., 1999). This result makes clear that there is not a marsh accretionary deficit at the Refuge related to insufficient mineral sediment supply, as observed at disturbed marsh locations (Boyd and Sommerfield, 2016). However, the relationship between accretion rate and marsh elevation change is inconclusive, because the accretion rates do not account for land subsidence due to sediment compaction or glacio-isostacy. A unit increase in marsh accretion may, in fact, represent little increase in surface elevation (if any) if the marsh landscape is subsiding at the same rate. Although surface elevation tables (SET) were recently installed at the Refuge, there is not yet an elevation record to establish rates of surface elevation change. Excluding the upland STEAM03, the marsh at all of the Refuge coring sites is accreting at or above local rates of RSL rise determine from tide gauges (3.4-3.5 mm/yr) (Figure 12). However, since a record of elevation change at the refuge has yet to be established, the actual relationship between marsh accretion and elevation change is unknown.

6.2 Spatial Variation in Accretion and Accumulation Rates

Marsh accretion rates vary widely within the Refuge. Based on the regression analysis, about 85% of the variation in accretion rate at Bombay Hook NWR can be

explained by variation in mineral sediment accumulation (Figure 15). In other words, aboveground processes of mineral sedimentation (sediment supply, canopy density, particle trapping) play a larger role in moderating accretion rates than belowground processes (root-rhizome productivity, biomass formation). Previous research by Pethick (1981) suggests that the depth and duration of tidal flooding at a location promote the sedimentation of allochthonous sediment by settling. In studies of marsh transects, spatial variability has been widely documented with channel-adjacent sites having a higher sediment availability, and thus sediment accumulation rate, than interior marsh areas (DeLaune et al., 1983; Hatton et al., 1983, Stoddart et al., 1989). However, in this study, no refuge-scale relationship between radionuclide-derived sediment accumulation rate and core site elevation was observed (R^2=.05), and there were no relationships between the sediment accumulation rate distance to nearest waterway channel.

The variability of sediment accumulation rates, soil physical properties, and marsh accretion rates at Bombay Hook NWR is high. Generally, accretion rates are highest near Sluice Ditch and Money Marsh. For example, INT1, the core closest to Money Marsh has an accretion rate of 1.33 ± 0.06 cm/yr (^{210}Pb), whereas the three cores taken along Sluice Ditch have accretion rates above 0.8 cm/yr. The high rates of mineral sedimentation and accretion along Sluice Ditch (SD1, SD2, and LTHB4B) may be caused by their proximity to the sediment-rich Delaware Bay. Site INT1, on the other hand, may be receiving elevated sedimentation rates due to its location southwest of the Money Marsh pools. Preliminary modelling of wind waves by Deb et al. (2016) over Money Marsh suggests that wave erosion may be a mechanism of pool widening,

thus site INT1 might be receiving sediment produced by wind wave erosion from the widening and deepening pool.

Site LTHB01, between Sluice Ditch and Money Marsh, is an exception to the high accretion rates measured in this area of the Refuge. Here the marsh has an accretion rate of 0.48 ± 0.02 cm/yr, which is well below that of neighboring low marsh core sites. At this site there was a drastic increase in mineral sediment accumulation at a soil depth of 30 cm or the year 1955 based on ^{210}Pb dating. Hence, the lower accretion rate at this site may be a response to a historical change in mineral sediment accumulation. More specifically, site LTHB01 may have experienced a brief vegetation die-off and repopulation as there is a distinct lack of observed root material at approximately 30 cm depth. This die-off would have temporarily reduced the platform's ability to trap sediment by loss of the plant canopy, resulting in reduced sediment accumulation. Upon regrowth of the canopy, sediment accumulation would have increased because of increased sediment trapping.

6.3 Sediment Production by Marsh Edge Erosion

Mariotti and Carr (2014) and Reed (1989) identified marsh edge erosion as an important source of mineral sediment and particulate organic matter to interior marsh platform. In modelling studies linking horizontal marsh loss with vertical marsh accretion, Mariotti and Carr (2014) found that edge erosion can provide a short-term mechanism for marsh resilience, by providing sediment to the marsh platform in times of reduced external sediment input. To quantify the mass of internally produced sediment at the Refuge, the mass of mineral sediment accumulated on the marsh platform between 1961 (the year of the aerial survey) and present day was compared

with the mass of sediment lost through erosion along the shoreface, expansion of inland pools, and adjustment of waterway channels over the same time period.

The mass (kg) of marsh soil gained since 1961 was estimated by multiplying the mineral sediment inventory (kg/m^2) at coring sites by the current area of the marsh platform (m^2). The sediment inventory is the product of the mineral sediment accumulation rate (derived from MA_{min} in Table 3 and converted to kg/m^2/y) and the number of years between 1961 and the year of core sampling (y). To improve the accuracy of the calculation, the marsh area was binned into high and low marsh zones (as shown in Figure 3), with *Phragmites* marsh considered high marsh, multiplied by mean sediment inventories of 137 kg/m^2 and 45 kg/m^2, respectively.

The volume of marsh soil lost since 1961 was calculated by multiplying the area of marsh platform loss (Table 2, Figure 6) by a representative soil column height (Table 4). Marsh loss due to inland pool formation was separated into either high marsh or low marsh pools by the surrounding vegetation. Pools surrounded by low marsh vegetation were, on average, deeper and thus were assigned a larger column of lost soil (1 m compared to 0.5 m). Soil loss due to shoreface erosion was assumed to remove a soil column that approximates the spring tide range (2 m), whereas loss along tidal channels were assumed to remove a 1 m column. To estimate the corresponding loss of mineral sediment mass, the soil volumes were multiplied by a mean mineral concentration for high marsh (190 kg/m^3) and low marsh (360 kg/m^3) soils based on the core physical properties data.

Over the past 55 years the mass of mineral sediment added to the marsh platform was an estimated 3.55×10^9 kg, whereas the amount lost was 3.2×10^9 kg. If these values are considered equivalent given the large uncertainties involved, then it

would appear that the marsh sedimentary system is more-or-less balanced despite the extent of marsh edge erosion. Hence, this result argues against the hypothesis that there is a deficiency in sediment supply to Refuge marshes. Moreover it suggest that, even if there were no external inputs of mineral sediment from the Refuge watershed or Delaware Bay, sediment produced internally by edge erosion could sustain the measured rate of marsh sediment accumulation.

6.4 Spatial Variability of Salt Marsh Platform Loss

Over the past ~50 years shoreline erosion and inland pool formation and expansion have been the main modes of marsh loss at Bombay Hook NWR. Shoreline erosion, responsible for ~35% of the lost marsh area, is most active in the southern half of the refuge, while inland pool expansion, responsible for ~50% of the marsh loss, is most pronounced in the northern half. This pattern of marsh loss may be related to the extrinsic processes associated with estuarine transgression. A wave model developed by Chen et al. (2017) concludes that northerly and southerly winds cause the most powerful waves in the Delaware Estuary. The shoreface of the Refuge between the Leipsic and Mahon Rivers protrudes into the Delaware Bay, exposing it to waves from both dominant directions. At the same time, the Refuge shoreface north of the Leipsic River may be protected from waves generated from southerly winds, while the inverse is true for the shoreface south of the Mahon River. This wave climate would cause the southern shoreface of the Refuge to be subjected to a higher average yearly wave power, resulting in higher shoreline retreat rates.

The expansion of large inland pools is concentrated in the northern half of the refuge between the Leipsic River and Sluice Ditch. Previous studies have demonstrated that pools can form as a result of disturbances that stress vegetation, and expand

through biogeochemical processes that reduce or preclude production of belowground biomass, or physical processes such as ice rafting or wrack deposition (Redfield, 1972; van Huissteden and van de Plassche, 1998; Mariotti, 2016). Some studies have alluded to waterlogging following storms or land subsidence as culprits for pool formation (Warren and Niering, 1993; Kelley et al., 1995; Hartig et al., 2002). Although the initiation and expansion of pooling at the Refuge is unknown, results of this study strongly suggest that a marsh accretionary deficit related to low mineral sediment supply can be ruled out.

As observed in many North American coastal marshes (e.g., Jefferies et al., 2003), goose herbivory is a cause of vegetation stress at the Refuge. Previous studies at the Refuge have demonstrated that goose herbivory and marsh loss have coincided in the past (Young, 1985), yet more recent work suggests that the marshes within the Refuge and elsewhere in the mid-Atlantic region are able to quickly recover and even gain vegetated platform area, despite increased grazing rate from growing geese populations (Smith, 1994). This indicates that herbivory is most likely a secondary stressor and not the primary cause of pooling.

Wilson et al. (2014) proposed that the formation of inland pools may be related to the drainage density of the salt marsh complex. Drainage density in a salt marsh is calculated by dividing total channel length of all creeks and rivers within a marsh complex subbasin by the total subbasin area. Mariani et al. (2003) found that the channel length of salt marsh basins within the Venice Lagoon are defined by basin area. They also observed a correlation between channel length and tidal prism volume, however, this relationship differed among basins. From these two relationships, they suggest that a salt marsh channel configuration is “frozen” once the marsh platform

develops vegetation and can only undergo minor changes in response to future hydrodynamic forcing.

In her study, Wilson et al. (2014) observed that pool surface area is inversely proportional to drainage density. They found that infilling of anthropogenically-ditched channels caused a decrease in the drainage density of a salt marsh in Plum Island Estuary. This channel-filling causes a three-fold increase in the area of high-marsh pools. In a different section of Plum Island, an increase in natural channel length caused the closing of low marsh pools. Wilson et al. (2014) proposed that the pool surface elevation plays a role in determining its capability for recovery. For example, if the pool surface is below mean sea level, vegetation will be unable to recolonize the platform and the pool may become a stable feature. If the pool surface elevation remains within a range conducive to vegetation, it may accrete very quickly (7-8 mm/yr) once revegetated (Kirwan and Gutensbergen, 2010).

At Bombay Hook NWR, the two largest marsh pools (Money Marsh and Leatherberry Fats) occur on a channel-connected low marsh platform directly adjacent to a managed freshwater impoundment, Shearness Pool. Construction of this impoundment in the 1930s may have shortened the drainage network for the northern marsh, which would have led to reduced drainage during spring tides and storm tides. Poor drainage could have led to waterlogging stress and die off in marshes immediately adjacent to the impoundment. Ongoing hydrodynamic studies and numerical modeling may offer insight into the processes behind this pooling at the Refuge (Abdolali et al., 2016). If this process is occurring at Money Marsh and Leatherberry Flats, geese herbivory may be slowing or preventing the recovery process but remain unrelated to initial pool formation.

6.5 Salt Marsh Loss and Estuarine Transgression

I hypothesize that the formation of inland pools in the Refuge is driven by a combination of natural (estuary transgression) and anthropogenic (marsh impoundment) factors that influence water exchanges between tidal waterways and marsh platform. In general, transgression is characterized by shoreface erosion and marsh loss on the seaward boundary as the shoreline migrates landward and upward, along with an increase in estuarine surface area. Estuary widening increases the tidal prism of the estuary provided the tidal range remains the same (Pethick and Lowe, 2000). The increase in estuarine tidal prism will extend into the salt marsh complex, because water levels within the marsh channels are driven by the rise and fall of coastal tides. The tidal prism of a salt marsh complex is contained within tidal channels most of the time (undermarsh tides), but extends over the marsh during spring tides and storm tides (overmarsh tides). During overmarsh tides, the water level within tidal channels increases, until all channels within the network are completely filled. This volume of water is known as the "bankfull tidal prism" of the marsh (Allen, 2000). When water height continues to increase, water floods low elevation marsh platforms adjacent to channels and creates the "overmarsh tidal prism". The size of this prism determines the flooding and inundation characteristics of the marsh platform, which may be better described by the term "hydraulic duty" (Allen, 1997). Hydraulic duty is calculated by dividing the overmarsh tidal prism by the catchment area, and describes the average difference between the mean marsh platform elevation and high water level.

In cases where the hydraulic duty is too large, the marsh platform may become "over-inundated" and drown vegetation, or the marsh complex may respond through increased connections to its creek network (Allen, 1997). Hydraulic duty may be limited by either reducing the overmarsh tidal prism (through lessening the overall tidal

prism or increasing the bankfull tidal prism) or increasing the surface area of the salt marsh. Thus, the lengthening, deepening, or widening of tidal creeks will reduce the amount of water needing to be drained from the marsh platform. Marsh platform accretion provides the dual benefit of maintaining a conducive elevation for plant survival, while increasing the elevation of the marsh platform relative to tidal channels, which contributes to an optimal balance between the bankfull and overmarsh tidal prism. The surface area of the marsh can be increased through upland migration, which may also permit the lengthening of tidal creeks.

Following the processes described above, the formation and growth of inland pools in the northern section of Bombay Hook NWR could be a response to an increase in hydraulic duty of the marsh. Specifically, there was a decrease in marsh surface area as a result of transgressive erosion of the estuary shoreface and marsh impoundment on the seaward and upland boundaries, respectively, but the tidal prism remained the same, at least temporarily. Since channel length (bankfull tidal prism) and salt marsh area would have both decreased during this period of marsh loss, the hydraulic duty would have increased, over-inundating the marsh platform. Moreover, the tide range may have even increased somewhat over the past several centuries as transgressive erosion destroyed the former confluence of the Leipsic and Simons Rivers, and created two tidal inlets from one. The former confluence would have presented more hydraulic resistance to the propagating oceanic tide, perhaps reducing the former tide range in the marsh interior. In response, areas of marsh platform connected to tidal creeks drowned, creating mudflats that flood during high tides and are left exposed during low tides, effectively increasing the bankfull tidal prism, and reducing the hydraulic duty. In summary, when landward migrating salt marshes encounter natural or anthropogenic

barriers, they lose their ability to increase their surface area to maintain an optimal hydraulic duty for drainage and plant growth.

Chapter 7

CONCLUSIONS

This study investigated the rates of accretion and mineral sediment accumulation at Bombay Hook NWR to determine whether vertical accretion at the Refuge is limited by insufficient mineral sediment supply. To accomplish this, a comparison of historical aerial photographs was undertaken to establish patterns and rates of marsh loss over the last ~50 years. ^{137}Cs and ^{210}Pb chronologies were developed for 19 marsh sites throughout the Refuge to measure rates of mineral sediment and organic matter accumulation (mass/area/time) and vertical accretion (length/time) of the current marsh complex. The major conclusions of this study are listed below:

1. Between 1961 and 2012, Bombay Hook NWR lost ~8.6 million m^2 of marsh area. This constitutes ~20% of the 1961 marsh platform area.
2. Approximately 50% of the marsh loss was caused by the formation and expansion of inland pools. Shoreface erosion along the Delaware Bay boundary accounted for ~35% of the total loss and waterway channel widening and migration contributed ~15%. Marsh loss by shoreface erosion was concentrated in the southern section of the complex, while inland pool expansion centered in the northern section, adjacent to three freshwater impoundments.
3. Salt marsh accretion and mass accumulation rates measured for this study fall within the middle to upper range of similarly determined rates for undisturbed marshes of the Delaware Estuary. The depths of the ^{137}Cs activity peaks ranged from 9 to 45 cm, equating to accretion rates

between 0.17 ± 0.10 and 0.92 ± 0.02 cm/yr with an overall mean of 0.5 ± 0.13 cm/yr. In all cases the ^{137}Cs peaks were distinct suggesting that they had not been subjected to significant biological mixing. Accretion rates calculated using ^{210}Pb ranged from 0.29 ± 0.2 to 1.33 ± 0.06 cm/yr with an overall mean of 0.63 ± 0.33 cm/yr. Although there can be methodological differences in measured accretion rates, there was no difference between the means of the ^{137}Cs and ^{210}Pb rates measured in this study.

4. Mineral and organic mass accumulation rates correlated strongly with rates of accretion (R^2= .85 and .79 respectively), revealing that both mineral sediment and organic matter drive marsh accretion at the Refuge, and that belowground biomass accumulation and aboveground mineral sediment deposition set the minimum and maximum rates of accretion, respectively.
5. Marsh accretion rates measured in this study met or exceeded the rate of relative sea-level rise for the middle Delaware Estuary, based on the NOAA tide gauge record for Reedy Point (0.35 ± 0.05 mm/yr, 1956-2015).

This study concludes that the current marsh complex at Bombay Hook NWR is not experiencing an accretionary deficit related to insufficient mineral sediment supply. Furthermore, the marsh soil record provides no evidence of changing sedimentary conditions over the past 50-80 years. While recent marsh loss along the shoreface can be attributed to high wave energy in the Delaware Bay, the expansion of inland pools in the northern section of the Refuge in the past 75 years remains a mystery. This study

suggests that neither marsh accretion rates nor insufficient mineral sediment supply are causes of pool formation. Additional research on historical changes in tidal inundation, marsh accretion, and elevation change is needed to better understand the nature of pool expansion and marsh loss at the Refuge.

TABLES

Table 1: Core locations, elevations, dominant vegetation type, and core-averaged dry bulk density. Stars (*) designate elevations that were extracted from corrected LiDAR (Abdolali et al., 2016), while the rest were assumed to be the same elevation as a nearby Surface Elevation Table.

Core Id	Longitude (˚W)	Latitude (˚N)	Elevation (m) (NAVD88)	Vegetation Type	Dry Bulk Density (g/cm^3)
AF02A	75.4109	39.1995	1.07	*S. alterniflora*	0.45 ± 0.08
BHIN01	75.4248	39.2628	0.89	*S. patens*	0.19 ± 0.03
BHIN03C	75.4302	39.2837	0.72	*S. patens*	0.33 ± 0.06
BHIS02C	75.4101	39.2618	0.88	*S. patens*	0.34 ± 0.06
GI01	75.4291	39.2523	0.74	Mixed	0.18 ± 0.02
GI03	75.4589	39.2609	0.65	*S. alterniflora*	0.32 ± 0.04
INT1	75.4624	39.2670	0.70*	*S. alterniflora*	0.44 ± 0.04
INT2	75.4488	39.2438	0.81*	*S. patens*	0.35 ± 0.07
INT3	75.4295	39.2580	0.60*	*S. patens*	0.25 ± 0.04
KELL03	75.4029	39.1989	1.22	*S. patens*	0.28 ± 0.05
KENT01	75.4566	39.2383	0.78	Mixed	0.31 ± 0.03
KENTBS	75.4084	39.2278	1.01*	*S. patens*	0.32 ± 0.09
KENTNEW	75.4538	39.2298	0.57*	*S. alterniflora*	0.41 ± 0.03
KENTNS	75.4348	39.2233	0.98*	*S. alterniflora*	0.49 ± 0.05
LTHB01	75.4604	39.2816	0.71*	*S. alterniflora*	0.30 ± 0.14
LTHB4B	75.4521	39.2939	0.88*	*S. alterniflora*	0.51 ± 0.05
SD1	75.4620	39.2900	0.78*	*S. alterniflora*	0.49 ± 0.03
SD2	75.4436	39.2946	0.81*	*S. alterniflora*	0.53 ± 0.04
STEAM03	75.4549	39.2080	0.91	Mixed	0.43 ± 0.06

Table 2: Change in salt marsh platform area between 1961 and 2012. The area of marsh loss was broken down into four categories as described in the text.

Year	**Marsh Area (m^2)**	**Error (m^2)**	**Percentage Change**	**Error Percentage**
1961	47,935,998	2,713,691		5.7%
2012	39,330,816	1,609,825		4.1%
Change	**-8,605,182**	**3,155,259**	**18.0%**	**6.6%**
Classification Zone	**Marsh Loss (m^2)**	**Marsh Gain (m^2)**	**Net Change (m^2)**	**% of Change**
Channel	1,775,708	208,175	-1,567,534	20%
Inland Pool	4,372,233	227,031	-4,145,202	50%
Shoreline	3,029,745	2,510	-3,027,235	35%
Upland	11,976	146,766	134,789	0%

Table 3: Radionuclide inventories (INV), marsh accretion rates (AR), and mass accumulation rates (MAR) for core sites at Bombay Hook NWR. Also shown is the amount of mineral sediment (MA_{min}) and organic matter (MA_{org}) accumulated above the 1963 peak depth. Stars (*) designate incomplete radionuclide inventories. Double stars (**) indicate accumulation derived from ^{210}Pb chronology instead of the ^{137}Cs peak.

Core ID	^{137}Cs INV (mBq/cm^2)	^{137}Cs AR (cm/yr)	^{137}Cs MAR (g/cm^2/yr)	^{137}Cs MA_{org} (g/cm^2)	^{137}Cs MA_{min} (g/cm^2)	^{210}Pb INV (mBq/cm^2)	^{210}Pb AR (cm/yr)	^{210}Pb MAR (g/cm^2/yr)
AF02A	128.1 ± 8.4*	0.52 ± 0.02	0.25	2.8	10.4	915.1 ± 46.7	0.61 ± 0.07	0.29
BHIN01	102.3 ± 6.1	0.37 ± 0.02	0.08	2.0	2.2	438.7 ± 28.9	0.34 ± 0.08	0.08
BHIN03C	150.5 ± 8.2	0.43 ± 0.02	0.12	2.0	4.4	547.2 ± 47.6	0.35 ± 0.07	0.10
BHIS02C	98.6 ± 9.2*	0.51 ± 0.02	0.17	2.5	6.2	1150.9 ± 84.5*	0.67 ± 0.08	0.22
GI01	156.1 ± 9.2	0.40 ± 0.02	0.08	1.9	2.1	493.0 ± 33.1	0.32 ± 0.11	0.06
GI03	146.0 ± 11.6*	0.63 ± 0.02	0.22	8.8	2.5	1204.3 ± 85.2*	1.07 ± 0.08	0.35
INT1	197.7 ± 21.7*	N/A	N/A	5.1**	26.6**	1468.4 ± 129.4*	1.33 ± 0.06	0.60
INT2	111.9 ± 9.4*	0.58 ± 0.02	0.22	3.5	8.0	1475.8 ± 76.9*	0.65 ± 0.11	0.23
INT3	88.4 ± 6.5	0.43 ± 0.02	0.11	2.6	3.4	700.2 ± 41.5	0.29 ± 0.20	0.09
KELL03	130.7 ± 6.6	0.33 ± 0.02	0.09	1.7	2.9	466.7 ± 30.1	0.33 ± 0.11	0.10
KENT01	125.5 ± 7.3	0.40 ± 0.02	0.13	2.4	4.3	511.1 ± 44.1	0.36 ± 0.07	0.11
KENTBS	120.4 ± 5.7	0.33 ± 0.02	0.10	2.0	3.1	555.4 ± 44.1	0.39 ± 0.06	0.12
KENTNEW	183.7 ± 14.9	0.79 ± 0.02	0.33	3.1	14.1	1008.6 ± 88.7	0.79 ± 0.06	0.34
KENTNS	119.4 ± 9.2	0.37 ± 0.02	0.18	2.5	6.8	888.1 ± 59.5	0.40 ± 0.06	0.20
LTHB01	119.2 ± 8.8	0.48 ± 0.02	0.21	2.2	8.8	544.7 ± 52.0	0.61 ± 0.07	0.23
LTHB4B	226.2 ± 22.4*	0.85 ± 0.06	0.46	3.5	20.7	1390.0 ± 134.3*	1.02 ± 0.07	0.55
SD1	235.8 ± 20.6*	N/A	N/A	4.2**	26.8**	1768.7 ± 164.1*	1.16 ± 0.15	0.59
SD2	204.9 ± 19.9	0.92 ± 0.02	0.50	3.7	23.0	1028.8 ± 95.5	0.92 ± 0.11	0.50
STEAM03	101.3 ± 7.3*	0.17±0.10	0.07	1.0	2.7	694.3 ± 76.0*	0.42 ± 0.09	0.19

Table 4: Calculation of mineral sediment gained through mineral sediment accumulation and lost through marsh platform erosion since 1961.

Gained through accretion	**Mean Sediment Inventory (kg/m^2)**	**Area (m^2)**	**Mineral Sediment Gained (kg)**
High Marsh	45	35% of 39,000,000	750,000,000
Low Marsh	137	55% of 39,000,000	3,000,000,000
Total			**3,550,000,000**

Lost through erosion	**Mineral Sediment Concentration (g/cm^3)**	**Vertical Loss (m)**	**Net Area (m^2)**	**Mineral Sediment Lost (kg)**
Low Marsh Pools	0.36	1	3,500,000	1,300,000,000
High Marsh Pools	0.19	0.5	600,000	69,000,000
Shoreline Change	0.19	2	3,000,000	1,500,000,000
Channel Adjustment	0.36	1	1,500,000	600,000,000
Total				**3,200,000,000**

FIGURES

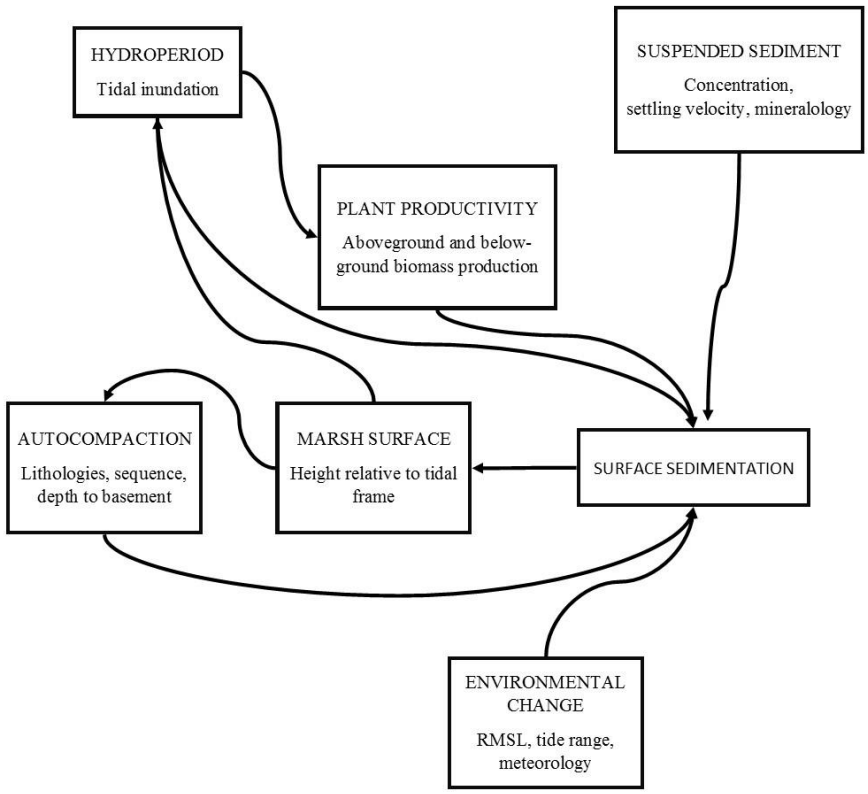

Figure 1: Conceptual model of feedbacks among tidal hydrodynamics, sediment supply, ecological processes, and marsh elevation gain. Modified from Allen (2000).

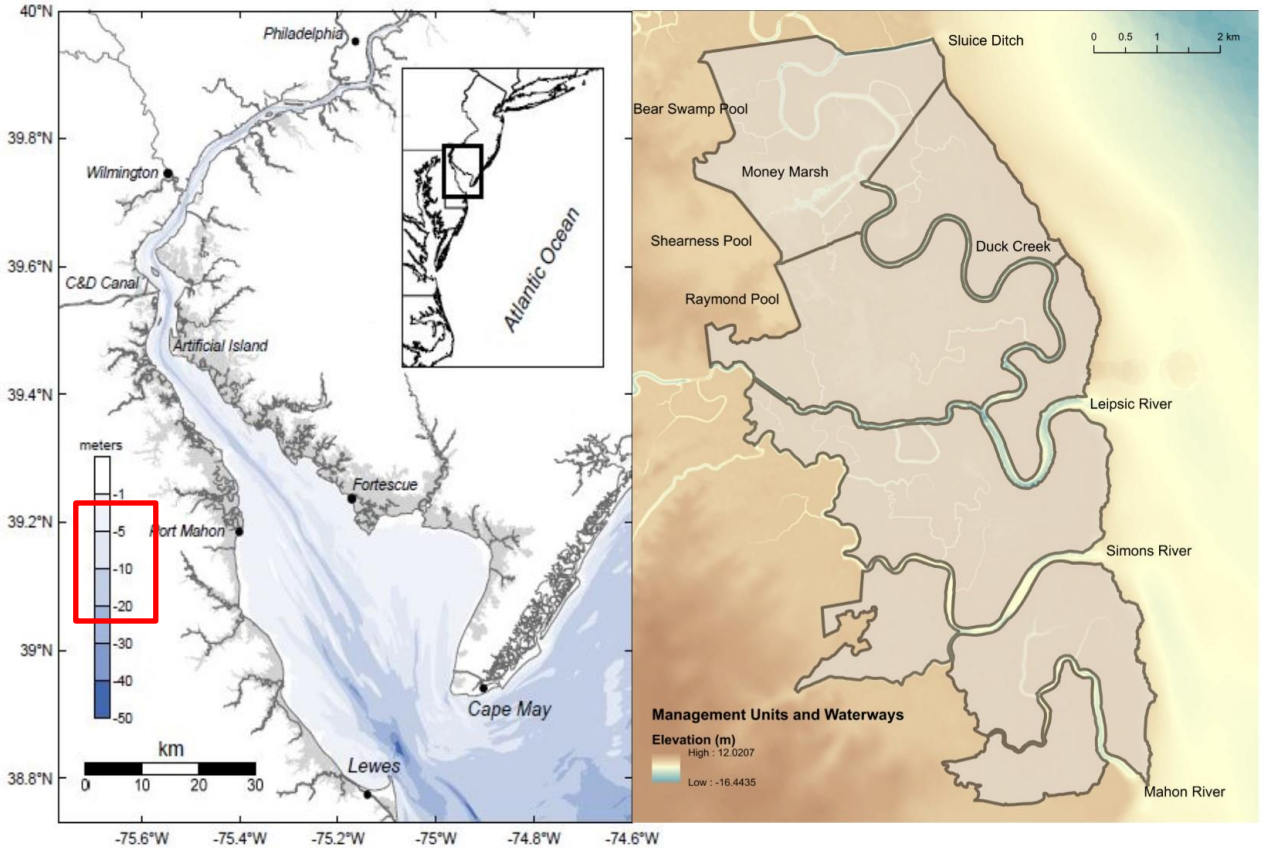

Figure 2: Location of Bombay Hook NWR within the Delaware Estuary (left panel, red box). The right panel is a LiDAR topographic map showing the salt marsh management units (black outlined boxes) and major waterways described in the text.

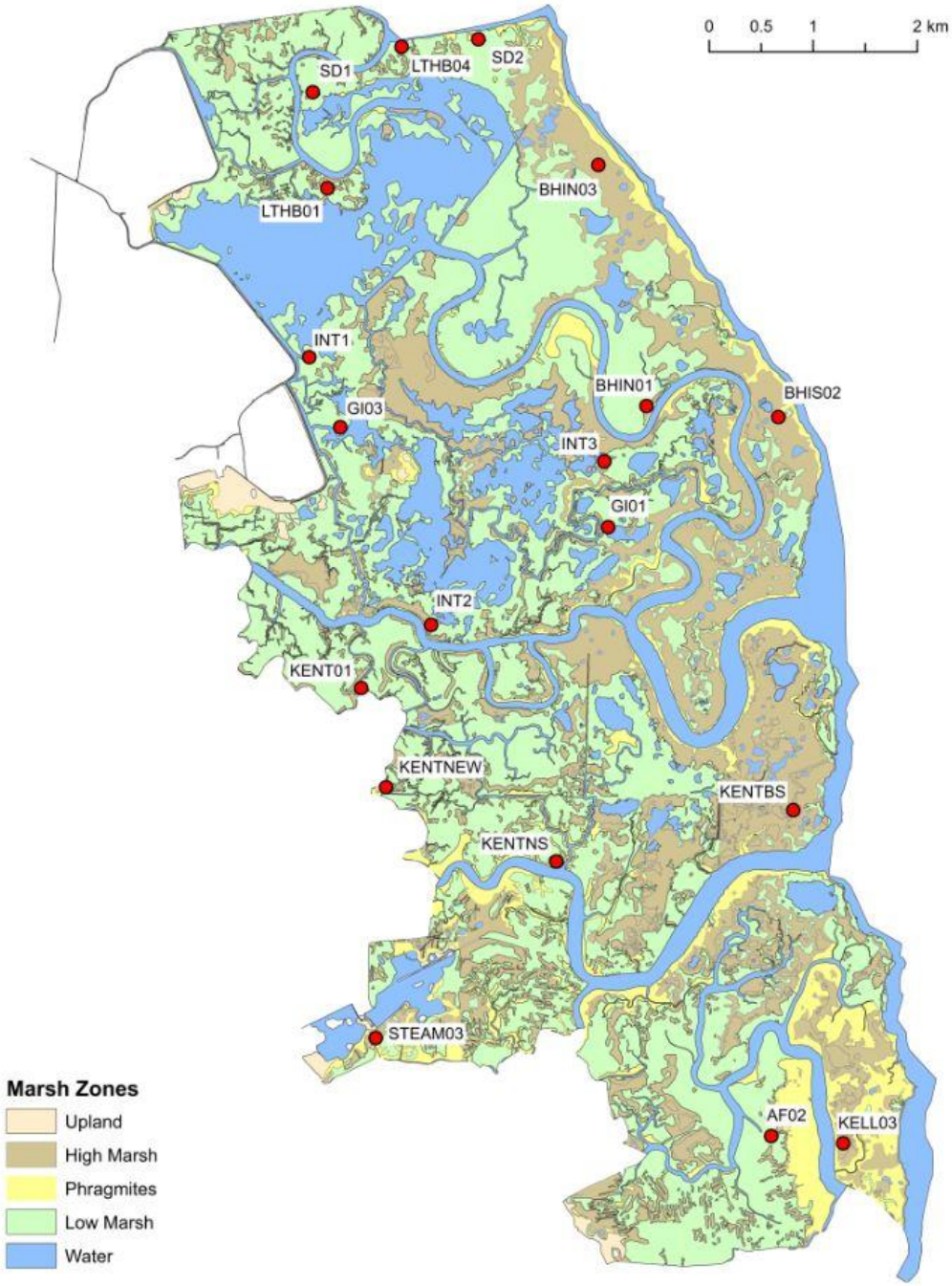

Figure 3: Map of salt marshes zones at the refuge based on dominant vegetation from a 2007 survey of vegetation by the USFWS. Brown (high marsh), yellow (high marsh), and green (low marsh) represent *Spartina patens*, *Phragmites australis*, and *Spartina alterniflora*, respectively. Red dots designate core locations.

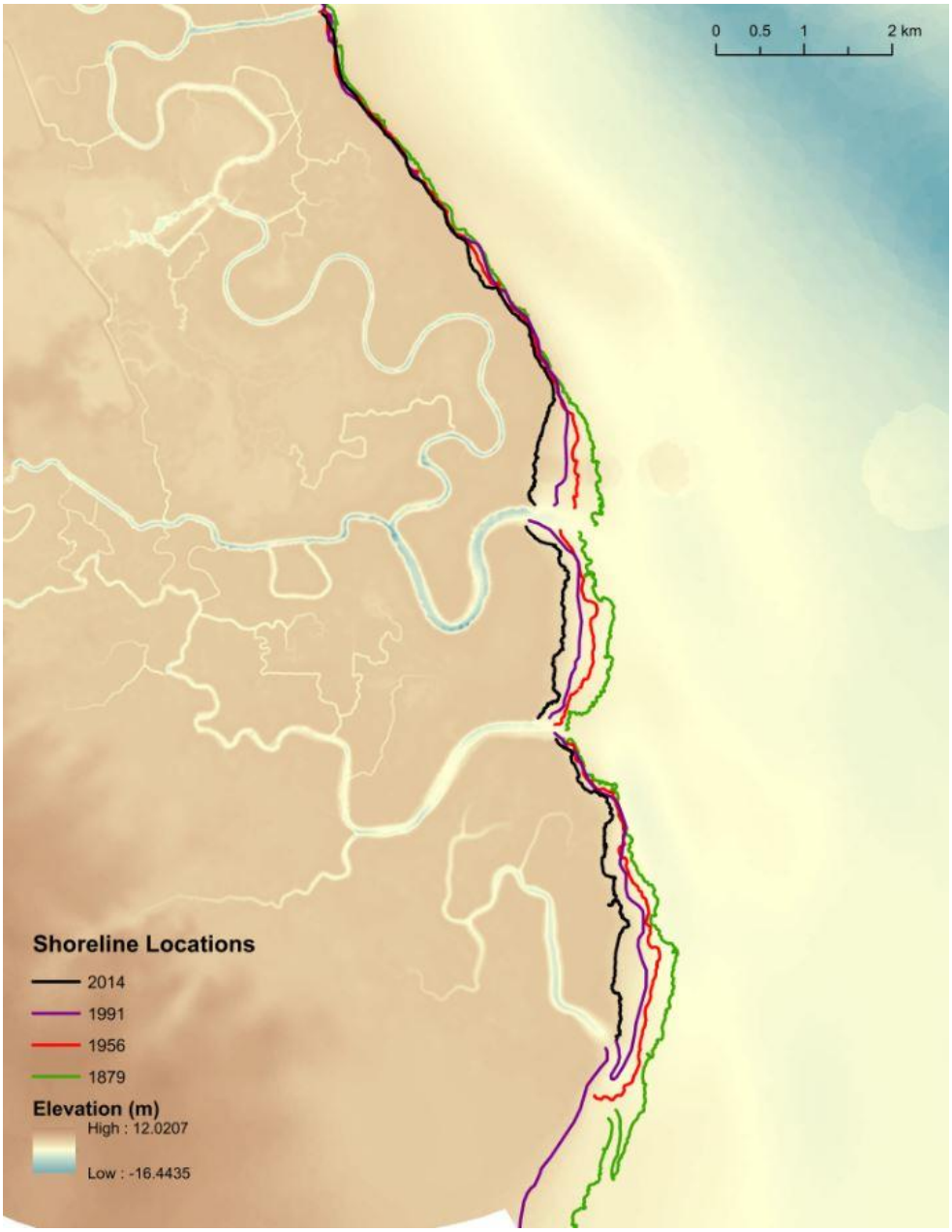

Figure 4: LiDAR elevation map of Bombay Hook NWR. LiDAR was corrected from a 2011 DNREC survey (DNREC, 2012). Notice that the main waterway channels are deep (up to 15 m), whereas pools and minor channels on the marsh platform are shallow (0.5 - 3m). Also shown are the former positions of the shoreline since 1879 (from Pijanowski, 2016).

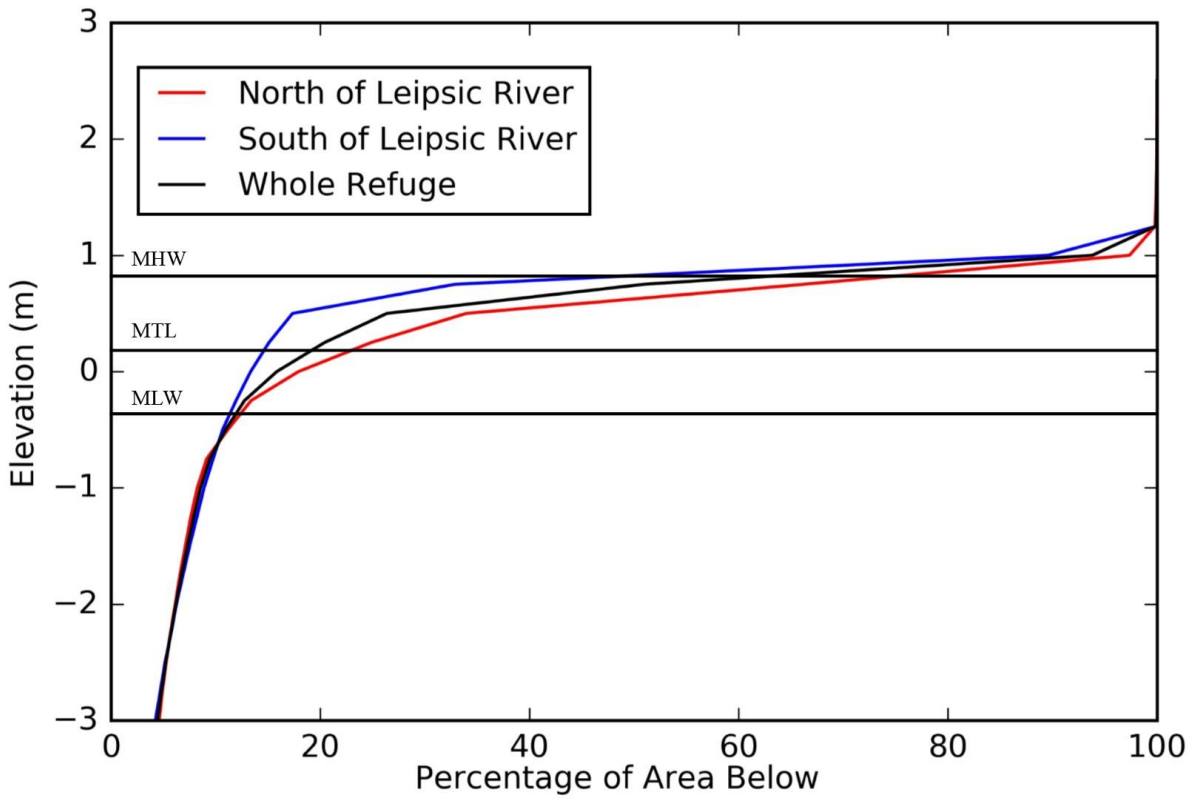

Figure 5: Hypsometric curves for the refuge based on analysis of LiDAR topography described in the text. The MHW, MTL, and MLW tidal datums shown were computed from DNREC water level data available for the northern part of the refuge.

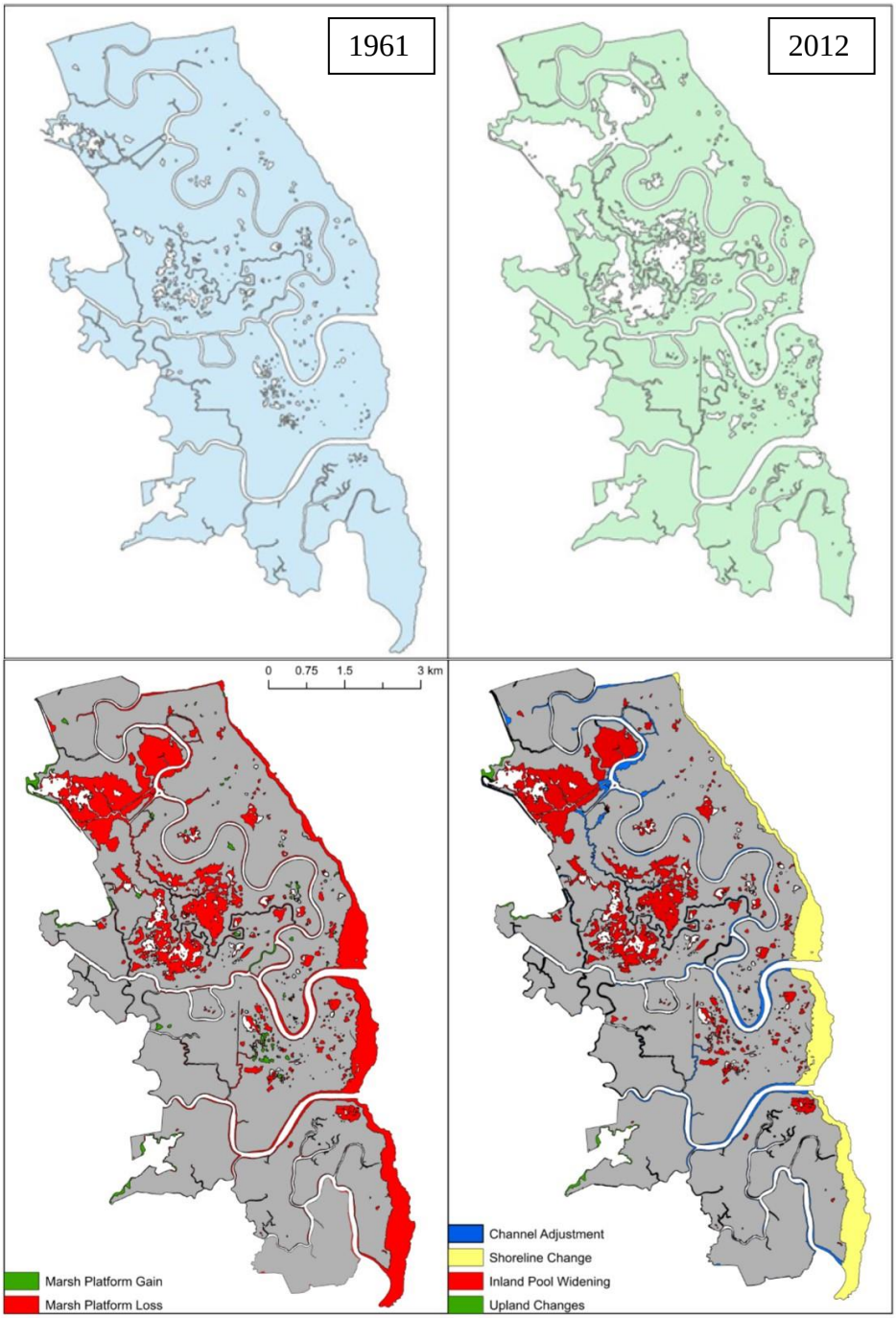

Figure 6: (Top) areal extent of the Bombay Hook NWR salt marsh in 1961 and 2012. (Bottom) Classified areas of marsh gain and loss between 1961 and 2012. See text for interpretation.

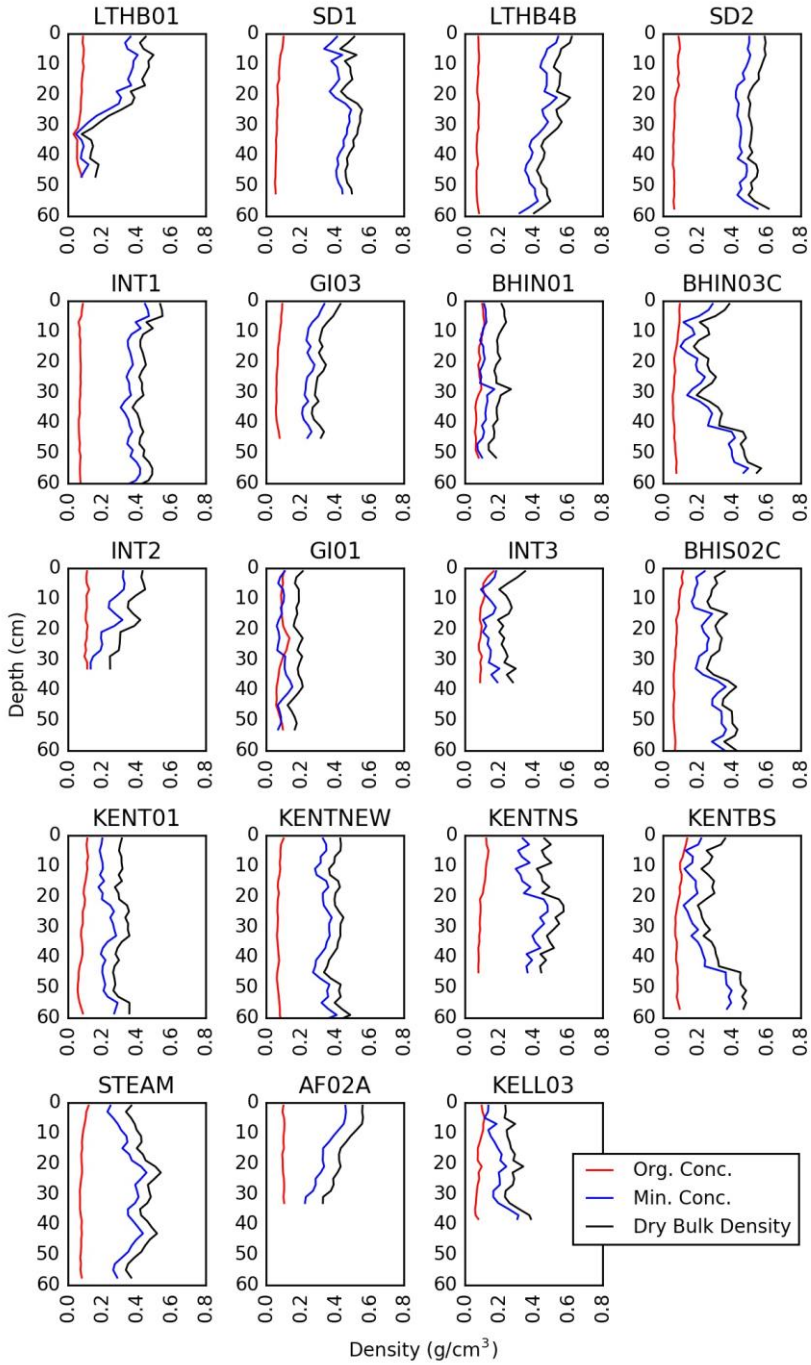

Figure 7: Depth profiles of sediment dry bulk density for the marsh cores. Using methods described in the text, dry bulk density was apportioned into mineral sediment and organic matter components.

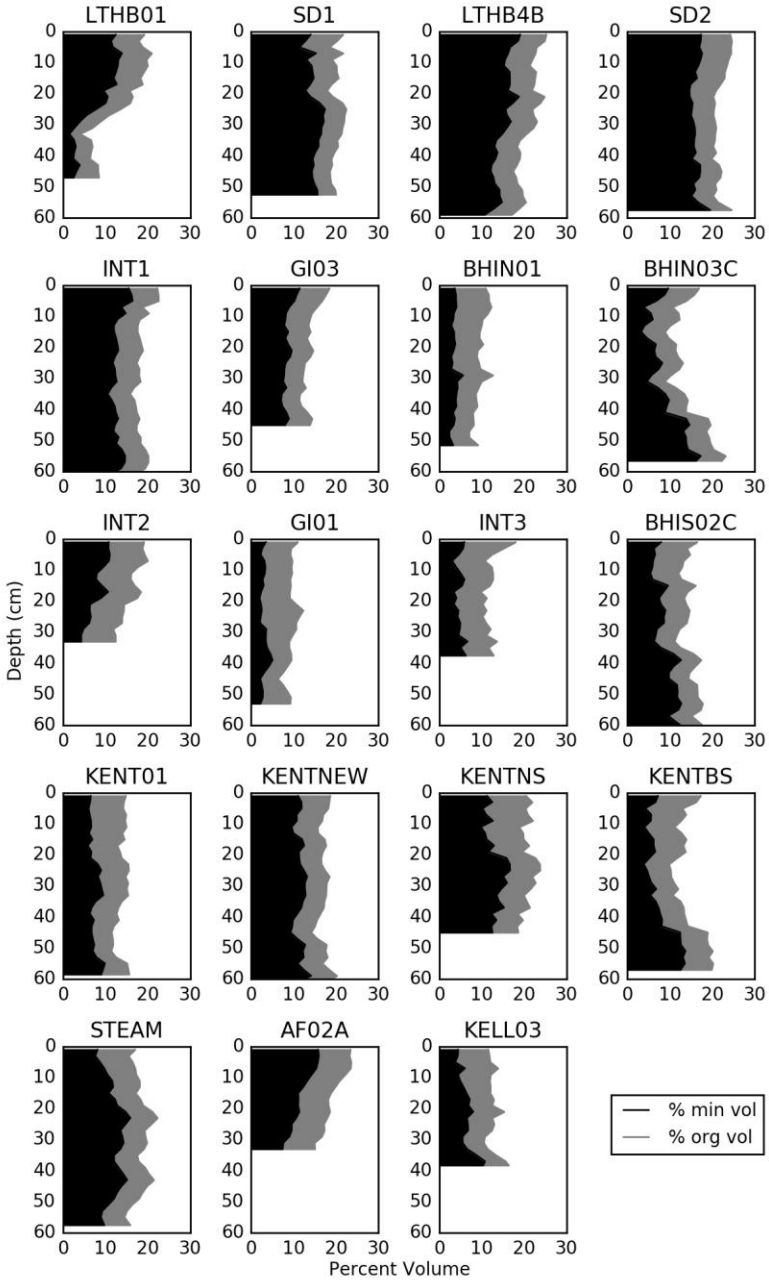

Figure 8: Depth profiles soil volume composition of the marsh cores. See text for methodology and interpretation.

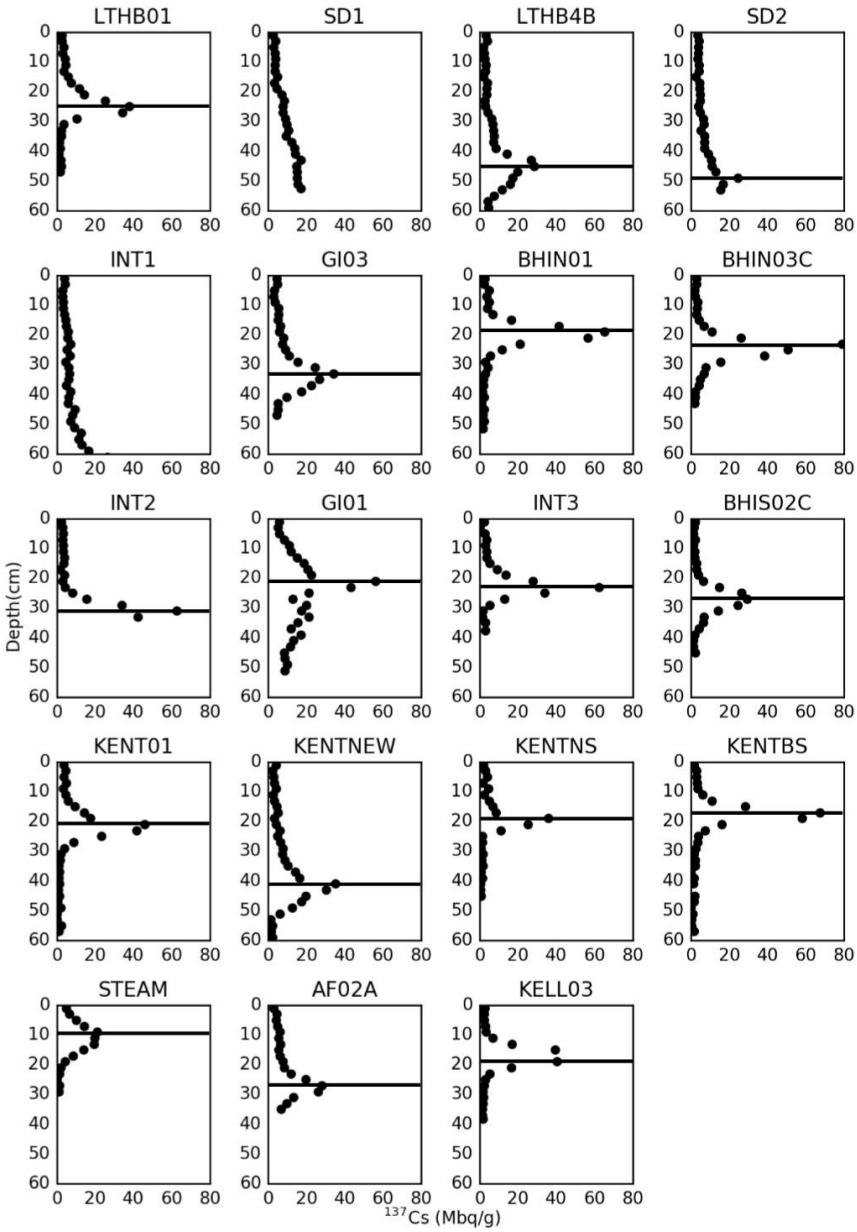

Figure 9: Depth profiles of ^{137}Cs activity for the marsh cores. The solid horizontal line marks the depth of the activity peak concordant with 1963-1964. See Table 3 for the corresponding accretion rates and the text for interpretation of data.

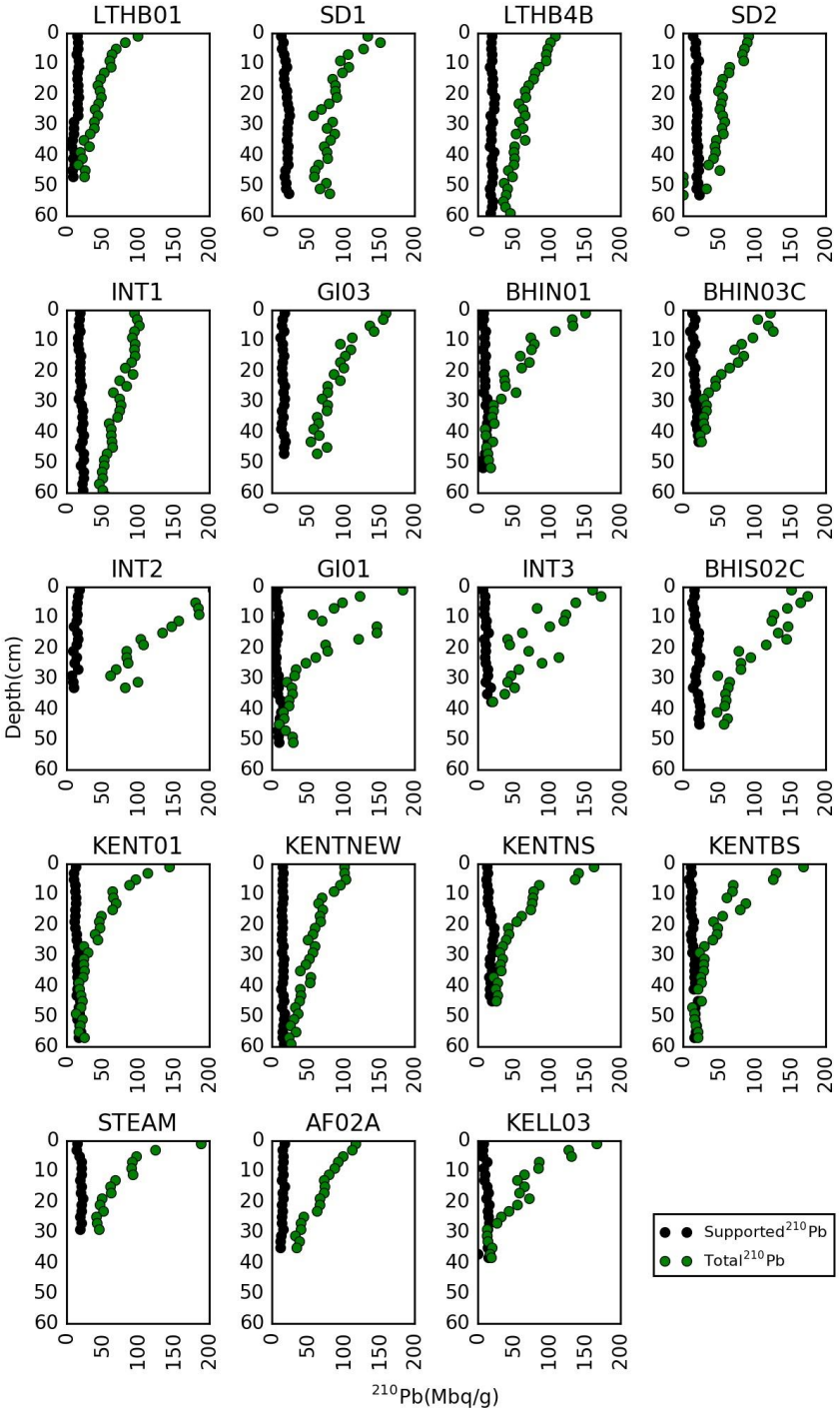

Figure 10: Depth profiles of supported ^{210}Pb (black) from ^{210}Bi activity and total ^{210}Pb (green) for the marsh cores.

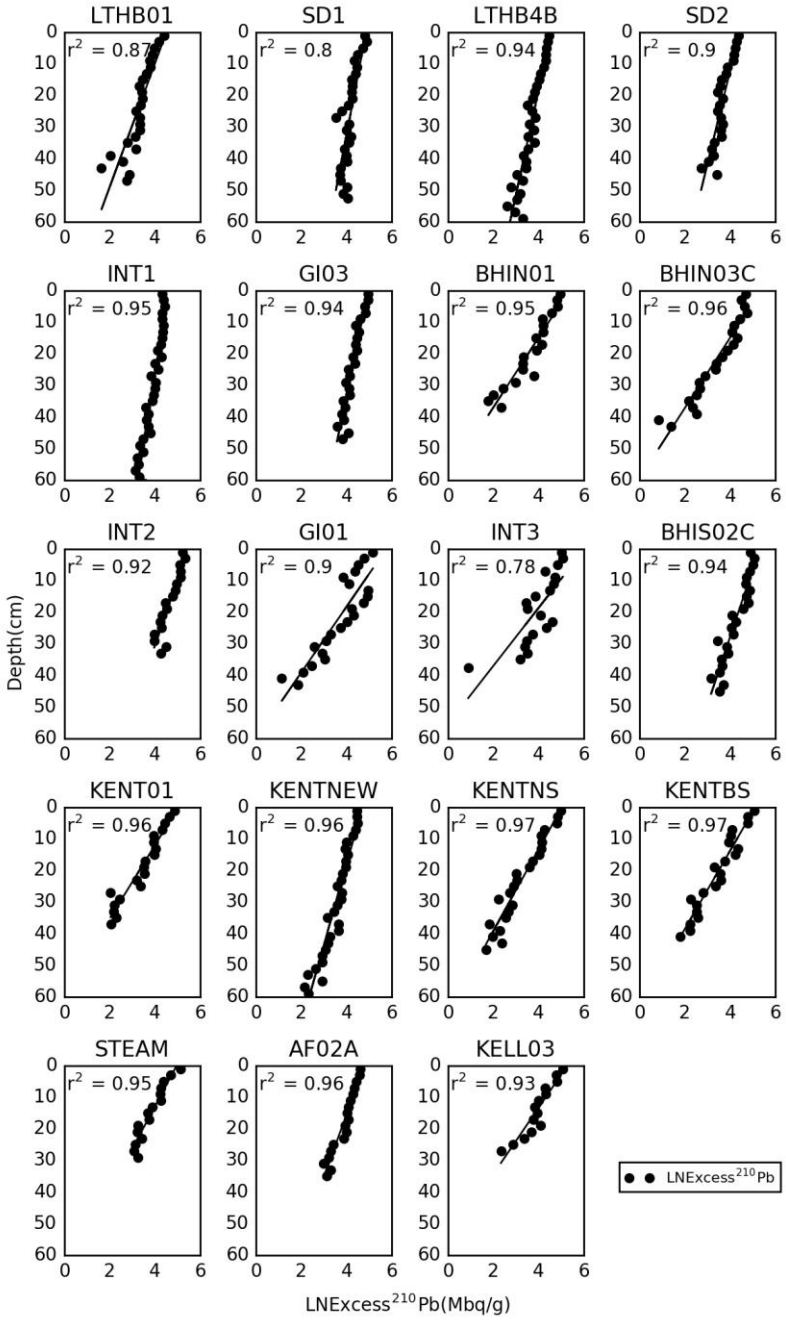

Figure 11: Depth profiles of the natural log of $^{210}Pb_{xs}$ activity. The solid line is the regression used to calculate the CFCS accretion rate (see Eq. 7).

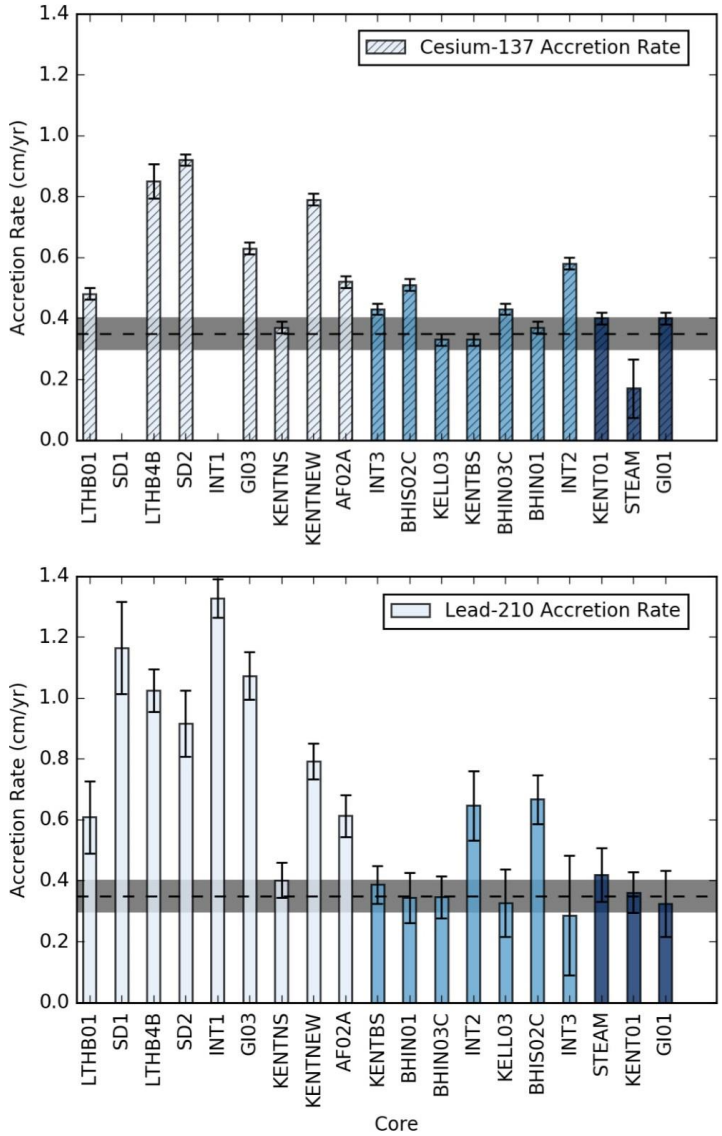

Figure 12: Cesium-137 and ^{210}Pb accretion rates for the marsh coring sites. Cesium-137 derived accretion rates are shown in the top graph and ^{210}Pb-derived rates are shown in the bottom graph. Bar color represents dominant vegetation at the coring site: dark blue=mixed *S. alterniflora* and *S. patens*; teal=*S. patens*; grey=*S. alterniflora*. The dotted horizontal line is the mean rate of relative SLR at the Reedy Point tide gauge (1956-2015) with the uncertainty range in grey.

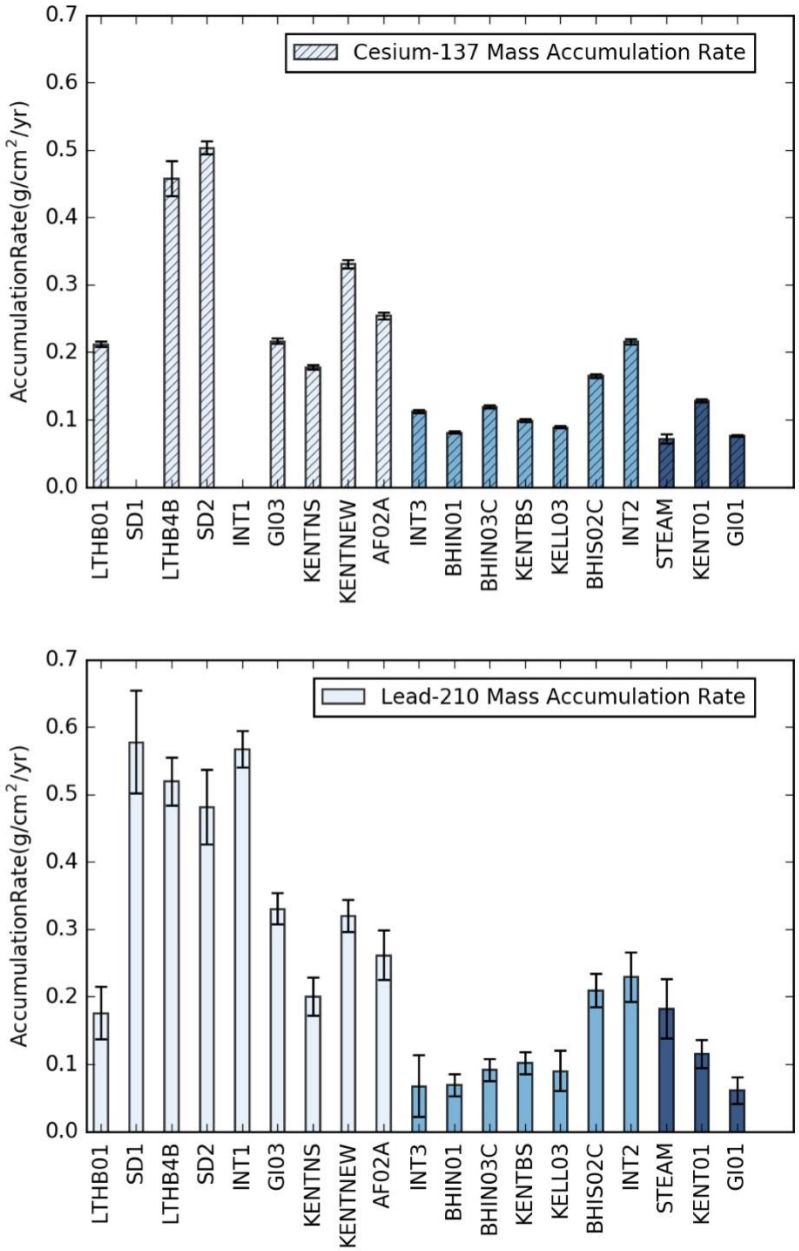

Figure 13: Cesium-137-derived mass accumulation rates (top) and ^{210}Pb-derived mass accumulation rates (bottom) for the marsh cores in this study. See the Figure 12 caption for the color designations.

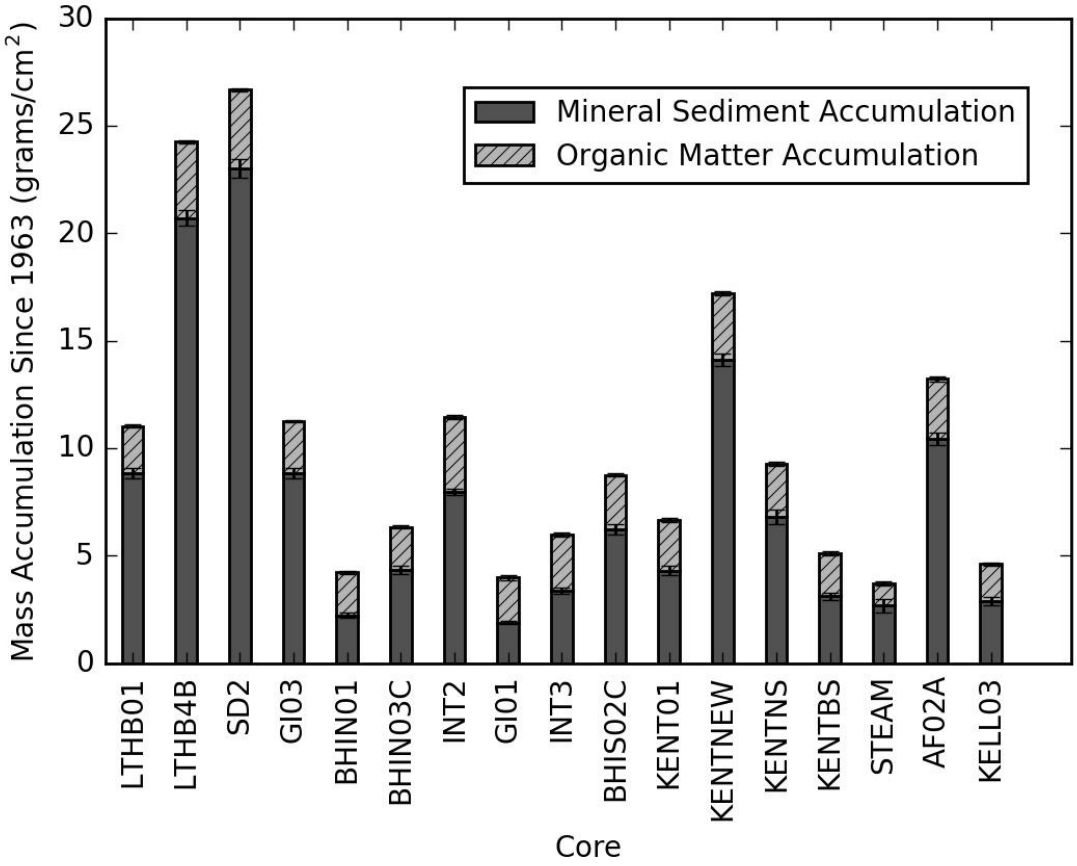

Figure 14: Stacked bar plot of mineral sediment and organic matter accumulation at the coring sites since 1963, based in the depth of the ^{137}Cs peak in the marsh soil. Note that the mass of mineral sediment accumulation is larger than organic matter at most sites. See text for further interpretation.

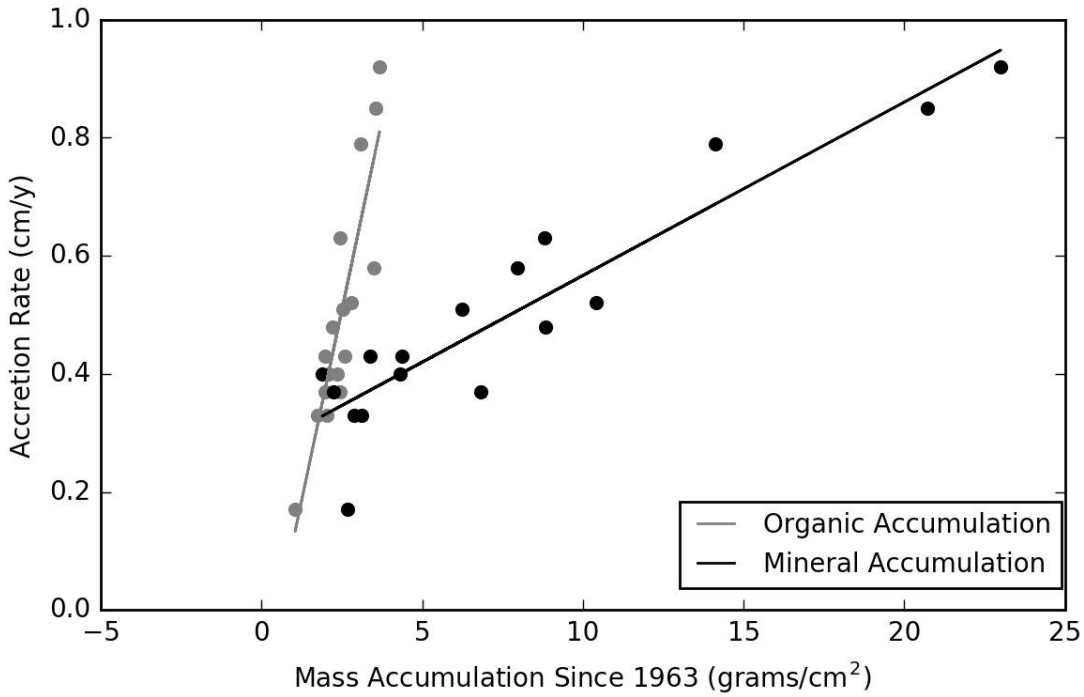

Figure 15: Scatter plot of ^{137}Cs-derived accretion rate versus organic matter (grey) and mineral sediment (black) mass accumulated since 1963 (R^2= .79 and .85 respectively). Note that both mineral and organic components of the soil are strongly correlated with accretion rate.

REFERENCES

Abdolali, A., J., Kirby, J.T., Shi, F. and Guiteras, S., 2016. "Field and modeling studies of salt marshes in Bombay Hook National Wildlife Refuge in Delaware". Restore America's Estuaries, 8th National Summit on Coastal and Estuarine Restoration and 25th Biennial Meeting of The Coastal Society, New Orleans, LA, USA.

Allen, J.R.L., 1997. Simulation models of salt-marsh morphodynamics: Some implications for high-intertidal sediment couplets related to sea-level change. Sedimentary Geology, 113: 211-223.

Allen, J.R.L., 2000. Morphodynamics of Holocene salt marshes: a review sketch from the Atlantic and Southern North Sea coasts of Europe. Quaternary Science Reviews, 19: 1155-1231.

Anisfeld, S.C., Tobin, M.J., and Benoit, G., 1999. Sedimentation rates in flow-restricted and restored salt marshes in Long Island Sound. Estuaries, 22(2): 231-244, doi:10.2307/1352980.

Appleby, P. G., and Oldfield, F., 1992. Application of lead-210 to sedimentation studies, in Ivanovich, M., and Harmon, R. S., eds., Uranium-series disequilibrium; applications to Earth, marine, and environmental sciences: Oxford, Clarendon Press: 731-778.

Armento, T.V. and Woodwell, G.M., 1975 Sedimentation Rates in a Long Island Marsh Determined by ^{210}Pb Dating. Limnology and Oceanography, 20: 452-456.

Boyd, B.M. and Sommerfield, C.K., 2016. Marsh accretion and sediment accumulation in a managed tidal wetland complex of Delaware Bay. Ecological Engineering, 92: 37-46.

Boyd, B.M., Sommerfield, C.K., and Elsey-Quirk, T., 2017. Hydrogeomorphic influences on salt marsh sediment accumulation and accretion in two estuaries of the U.S. Mid-Atlantic coast. Marine Geology, 383: 132-145.

Bricker-Urso, S. Nixon, S.W., Cochran, J.K., Hirschberg, D.J., Hunt, C., 1989. Accretion Rates and Sediment Accumulation in Rhode Island Salt Marshes. Estuaries, 12: 300-317, doi:10.2307/1351908.

Cahoon, D.R., Lynch, J.C., Hensel, P.F., Boumans, R.M., Perez, B.C., Segura, B., and Day, Jr., J.W., 2002. High precision measurement of wetland sediment elevation: II. The rod surface elevation table. Journal of Sedimentary Research, 72: 734-739.

Cahoon, D.R. and Reed, D.J., 1995. Relationships among marsh surface topography, hydroperiod, and soil accretion in a deteriorating Louisiana salt marsh. J. Coastal Research, 11: 357-369.

Carey, W., 1996. Transgression of Delaware's fringing tidal salt marshes: surficial morphology, substrate stratigraphy, vertical accretion rates, and geometry of adjacent and antecedent surfaces. PhD Dissertation, University of Delaware, Newark, DE, 639 p.

Chen, J.-L., Ralston, D.K., Geyer, W.R., Sommerfield, C.K., and Chant, R.J., 2017. Wave energy generation and dissipation in the Delaware Estuary. Manuscript in review.

Coleman, J.M., Huh, O.K., and Braud Jr., D. 2008. Wetland loss in world deltas. Journal of Coastal Research, 24: 1-14.

Dalrymple, R.W., Zitlin, B.A., Boyd, R., 1992. Estuarine facies models: conceptual basis and stratigraphic implications. Journal of Sedimentary Petrology, 62: 1130-1146.

Darmody, R.G., Foss, J.E., 1979. Soil-landscape relationships of the tidal marshes of Maryland. Soil Science Society of America Journal, 43: 534-541.

Day, J.W., Kemp, G.P., Reed, D.J., Cahoon, D.R., Boumans, R.M., Suhayda, J.M., and Gambrell, R., 2011. Vegetation death and rapid loss of surface elevation in two contrasting Mississippi delta salt marshes: The role of sedimentation, autocompaction and sea-level rise. Ecological Engineering, 37: 229-240.

de Groot, A.V., Veeneklaas, R.M., Kuijper, D.P.J., and Bakker, J.P., 2011. Spatial patterns in accretion on barrier-island salt marshes. Geomorphology, 134: 280-296.

Deb, M., Abdolali, A., Kirby, J.T., and Shi, F. 2016. Modelling wind waves in a confined tidal flat area: Bombay Hook National Wildlife Refuge, Delaware. Delaware Wetlands Conference Biannual Meeting.

DeLaune, R.D., Baumann, R.H., Gosselink, J.G., 1983. Relationships among vertical accretion, coastal submergence, and erosion in a Louisiana gulf coast marsh. Journal of Sedimentary Petrology, 53: 147-157.

DeLaune, R.D., Nyman, J.A., and Patrick Jr., W.H., 1994. Peat Collapse, Ponding and Wetland Loss in a Rapidly Submerging Coastal Marsh. Journal of Coastal Research, 4: 1021-1030.

DeLaune, R.D., W. Patrick, and R. Buresh. 1978. Sedimentation rates determined by 137Cs dating in a rapidly accreting salt marsh. Nature, 275: 532-533.

Delaware Department of Natural Resources and Environmental Control (DNREC), 2012. 2011 Delaware Department of Natural Resources and Environmental Control (DNREC) Lidar: Bombay Hook National Wildlife Refuge (1m). https://coast.noaa.gov/htdata/lidar1_z/geoid12a/data/1172.

Delaware Department of Transportation (DELDOT), 1963, DELDOT Cultural Resources: Archaeology/Historic Preservation, 3 p. (http://www.deldot.gov/archaeology/historic_pres/annual_reports/pdf/1963/1963_mosquito.pdf)

Delaware Geological Survey, 2006a. Delaware 1961 Aerial Photography. http://demac.udel.edu.

Delaware Geological Survey, 2006b. Delaware 1968 Aerial Photography. http://demac.udel.edu.

Feagin, R.A., Lozada-Bernard, S.M., Ravens, T.M., Moller, I., Yeager, K.M., and Baird, A.H., 2009. Does vegetation prevent wave erosion of salt marsh edges? Proceedings of the National Academy of Sciences, 106: 10109-10113.

Federer, C.A., Turcotte, D.E. and Smith, C.T., 1993. The organic fraction-bulk density relationship and the expression of nutrient content in forest soils. Canadian Journal of Forest Research, 23(6): 1026-1032.

Fitzgerald, D. M., Fenster, M. S. Argow, B. A., and Buynevich, I. V., 2008. Coastal impacts due to sea-level rise. Annual Review of Earth Planetary Science, 36: 601-647.

Fletcher, C.H., Knebel, H.J., and Kraft, J.C., 1990. Holocene evolution of an estuarine coast and tidal wetlands. Geological Society of America Bulletin, 102: 283-297.

Fletcher, C.H., Knebel, H.J., and Kraft, J.C., 1992. Holocene depocenter migration and sediment accumulation in Delaware Bay: a submerging marginal marine sedimentary basin. Marine Geology, 103: 165-183.

French, J.R, 1993. Numerical modelling of vertical marsh growth and response to rising sea-level, Norfolk, UK. Earth Surface Processes and Landforms, 18: 63-81.

French, J.R., 2006. Tidal marsh sedimentation and resilience to environmental change: Exploratory modelling of tidal, sea-level and sediment supply forcing in predominantly allochthonous systems. Marine Geology, 235: 119–136.

French, J.R., Spencer, T., 1993. Dynamics of sedimentation in a tide-dominated backbarrier salt marsh, Norfolk, UK. Marine Geology, 110: 315-331.

French, J.R., Spencer, T., Murray, A.L., and Arnold, N.A., 1995. Geostatistical analysis of sediment deposition in two small tidal wetlands, Norfolk, UK. Journal of Coastal Research, 10: 308-321.

Gedan, K.B., Silliman, B.R., and Bertness, M.D., 2009. Centuries of human-driven change in salt marsh ecosystems. Annual Review of Marine Science, 1: 117-141.

Graustein, W.C. and Turekian, K.K., 1986. 210Pb and 137Cs in Air and Soils Measure the Rate and Vertical Profile of Aerosol Scavenging. Journal of Geophysical Research, 91: 14,355-14,366.

Hartig, E.K., Gornitz, V., Kolker, A., Mushacke, F., Fallon, D., 2002. Anthropogenic and climate-change impacts on salt marshes of Jamaica Bay, New York City. Wetlands, 22: 71-89.

Hatton, R.S., DeLaune, R.D., and Patrick Jr., W.H., 1983. Sedimentation, accretion and subsidence in marshes of Barataria Basin, Louisiana. Limnology and Oceanography, 25: 494-502.

Heiri, O., Lotter, A.F., and Lemcke, G., 2001. Loss on ignition as a method for estimating organic and carbonate content in sediments: reproducibility and comparability of results. Journal of Paleolimnology, 25: 101-110.

Holdahl, S.R., Morrison, N.L., 1974. Regional investigations of vertical crustal movements in the U.S., using precise relevelings and mareograph data. Tectonophysics, 23: 373-390.

Horton, B.P., Engelhart, S.E., Hill, D.F., Kemp, A.C., Nikitina, D., Miller, K.G., Peltier, W.R. 2013. Influence of tidal-range change and sediment compaction on Holocene relative sea-level change in New Jersey, USA. Journal of Quaternary Science, 28: 403-411.

Jefferies, R.L., Rockwell, R.F., and Abraham, K.F., 2003. The embarrassment of riches: agricultural food subsidies, high goose numbers, and loss of Arctic wetlands – a continuing saga. Environmental Review, 11: 193-232.

Kauffman, G., Homsey, A., Chatterson, S., Mcvey, E., & Mack, S., 2011. Economic Value of the Delaware Estuary Watershed. Comprehensive Report prepared for the Partnership for the Delaware Estuary, Inc. Institute for Public Administration School of Public Policy & Administration College of Arts and Sciences. University of Delaware, June 2011. http://www.ipa.udel.edu/publications/DelEstuaryValueReport.pdf.

Kearney, M.S., Grace, R.E., and Stevenson, J.C., 1988. Marsh loss in Nanticoke Estuary, Chesapeake Bay. Geographical Review, 78:205-220.

Kearney, M.S., Stevenson, J.C., and Ward, L.G., 1994. Spatial and Temporal Changes in Marsh Vertical Accretion Rates at Monie Bay: Implications for Sea-Level Rise. Journal of Coastal Research, 10: 1010-1020.

Kelley, J.T., Gehrels, W.R., Balknap, D.F., 1995. Late Holocene relative sea-level rise and the geological development of tidal marshes at Wells, Maine, USA. Journal of Coastal Research, 11: 136-153.

Kim, G., Hussain, N., Church, T.M., Carey, W.L., 1997. The fallout isotope ^{207}Bi in a Delaware salt marsh: a comparison with ^{210}Pb and ^{137}Cs as a geochronological tool. The Science of the Total Environment, 196: 31-41.

Kirwan, M.L. and Guntenspergen, G.R., 2010. Influence of tidal range on the stability of coastal marshland. Journal of Geophysical Research: Earth Science: 115 (F2).

Kirwan, M.L. and Megonigal, J.P., 2013. Tidal wetland stability in the face of human impacts and sea-level rise. Nature, 504: 53-60.

Kirwan, M.L., Temmerman, S., Skeehan, E.E., Guntenspergen, G.R., Fagherazzi, S., 2016. Overestimation of marsh vulnerability to sea level rise. Nature Climate Change, 6: 253-260, doi:10.1038/nclimate2909.

Knebel, H.J., Fletcher III, C.H., Kraft, J.C., 1988. Late Wisconsinan – Holocene paleogeography of Delaware Bay; A large coastal plain estuary. Marine Geology, 83: 115-133.

Kraft, J.C., Yi, H., and Khalequzzaman, M., 1992. Geologic and human factors in the decline of the tidal salt marsh lithosome: the Delaware estuary and Atlantic coastal zone. Sedimentary Geology, 80: 233-246.

Marani, M., Belluco, E., D'Alpaos, A., Defina, A., Lanzoni, S., and Rinaldo, A., 2003. On the drainage density of tidal networks. Water Resources Research, 39: 1944-1973.

Marani, M., D'Alpaos, A., Lanzoni, S., and Santalucia, M., 2011. Understanding and predicting wave erosion of marsh edges. Geophysical Research Letters, 38, doi:10.1029/2011GL048995.

Mariotti, G., 2016. Revisiting salt marsh resilience to sea level rise: Are ponds responsible for permanent land loss?, Journal of Geophysical Research: Earth Surface, 121: 1391-1407, doi:10.1002/2016JF003900.

Mariotti, G., and Carr, J., 2014. Dual role of salt marsh retreat: long-term loss and short-term resilience. Water Resources Research, 50: 2963–2974, doi:10.1002/2013WR014676.

Mariotti, G. and Fagherazzi, S., 2010. A numerical model for the coupled long-term evolution of salt marshes and tidal flats. Journal of Geophysical Research: Earth Surface: 115 (F1).

Mariotti, G. and Fagherazzi, S., 2013. Critical width of tidal flats triggers marsh collapse in the absence of sea-level rise. Proceedings of the National Academy of Science, 110: 5353-5356.

Möller, I., Kudella, M., Rupprecht, F., Spencer, T., Paul, M., van Wesenbeeck, B.K.,Wolters, G., Jensen, K., Bouma, T.J., Miranda-Lange, M., Schimmels, S., 2014. Wave attenuation over coastal salt marshes under storm conditions. Nature Geoscience, 7: 727-731.

Morris, J.T, Sundareshwar, P.V., Nietch, C.T., Kjerfve, B., and Cahoon, D.R., 2002. Responses of coastal wetlands to rising sea level. Ecology, 83(10): 2869-2877.

Nicholls, R.J., Wong, P.P., Burkett, V.R., Codignotto, J.O., Hay, J.E., McLean, R.F., Ragoonaden, S., and Woddroffe, C.D., 2007. Coastal systems and low-lying areas. Climate Change 2007: Impacts, Adaptation and Vulnerability. Contribution of Working Group II to the Fourth Assessment Report of the Intergovernmental Panel on Climate Change. M.L. Parry, O.F. Canziani, J.P. Palutikof, P.J. van der Linden, and C.E. Hanson, Eds., Cambridge University Press, Cambridge, UK, 315-356.

Nikitina, D., Kemp, A., Engelhart, S.E., Horton, B.P., Hill, D.F., Kopp, R.E., 2015. Sea-level change and subsidence in the Delaware Estuary during the last ~2200 years. Estuarine, Coastal and Shelf Science, 164: 506-519.

Nikitina, D., Pizzuto, J.E., Martin, R.E., and Hippensteel, S.P., 2003. Transgressive valley-fill stratigraphy and sea-level history of the Leipsic River, Bombay Hook National Wildlife Refuge, Delaware, U.S.A. in Micropaleontologic Proxies for Sea-level Change and Stratigraphic Discontinuties. SEPM Special Publication No. 75: 51-62.

Nyman, J. A., Walters, R. J., Delaune, R. D. & Patrick, W. H., 2006. Marsh vertical accretion via vegetative growth. Estuarine Coast. Shelf Science, 69: 370-380.

Orson, R., Panageotou, W., Leatherman, S.P., 1985. Response of Tidal Salt Marshes of the U.S. Atlantic and Gulf Coasts to Rising Sea Level. Journal for Coastal Research, 1: 29-39.

Pethick, J.S., 1974. The Distribution of Salt Pans on Tidal Salt Marshes. Journal of Biogeography, 1: 57-62.

Pethick, J.S., 1981. Long-term accretion rates on tidal salt marshes. Journal Sedimentary Petrology, 51: 0571–0577, doi:10.1306/212F7CDE-2B24-11D7-8648000102C1865D.

Pethick, J. and Lowe, J., 2000, Regime models in estuarine research. In EMPHASYS Consortium, A Guide to Prediction of Morphological Change within Estuarine Systems, HR Wallingford, TR114.

Phillips, J.D., 1986. Coastal submergence and marsh fringe erosion. Journal of Coastal Research, 2(4): 427-436.

Phillips, J.D., 1987. Shoreline processes and establishment of *Phragmites australis* in a coastal plain estuary. Vegetatio, 71: 139-144.

Pijanowski, K., 2016. Patterns and Rates of Historical Shoreline Change in the Delaware Estuary. MS Thesis, University of Delaware, Lewes, DE, 97 p.

Redfield, A.C., 1972. Development of a New England salt marsh. Ecological Monographs, 42(2): 201-237.

Reed, D. J., 1989, Patterns of sediment deposition in subsiding salt marshes, Terrebonne Bay, Louisiana: The role of winter storms. Estuaries, 12(4): 222-227.

Reed, D. J., 1995. The response of coastal marshes to sea-level rise: Survival or submergence? Earth Surface Processes and Landforms, 20: 39-48, doi:10.1002/esp.3290200105.

Reed, D.J, Bishara, D.A., Cahoon, D.R., Donnelly, J.P., Kearney, M.S., Kolker, A.S., Leonard, L.L., Orson, R.A., and Stevenson, J.C., 2008. Site-Specific scenarios for wetlands accretion as sea level rises in the mid-Atlantic region. Section 2.1. In :Titus, J.G., Strange, E.M. (Eds.), Background Documents Supporting Climate Change Science Program Synthesis and Assessment Product 4.1. EPA.

Robbins, J.A., 1978. Geochemical and geophysical applications of radioactive lead. In: Nriagu, J.O. (ed.), Biogeochemistry of Lead in the Environment, Elsevier, Amsterdam, Netherlands: 285-393.

Schuerch, M., Vafeidis, A., Slawig, T. and Temmerman, S., 2013. Modeling the influence of changing storm patterns on the ability of a salt marsh to keep pace with sea level rise. Journal of Geophysical Research, 118: 84-96.

Smith, F. 1994. Progress report no. 6 – Figures, tables, and maps (draft). U.S. Fish and Wildlife Service, Bombay Hook NWR, Smyrna, DE.

Sommerfield, C.K. and Wong, K.C., 2011. Mechanisms of sediment flux and turbidity maintenance in the Delaware Estuary. Journal of Geophysical Research, 116, 2156-2202.

Stoddart, D.R., Reed, D.J., and French, J.R., 1989. Understanding salt-marsh accretion, Scolt Head Island, Norfolk, England. Estuaries, 12: 228-236.

Stralberg, D. M. et al., 2011. Evaluating tidal marsh sustainability in the face of sea-level rise: a hybrid modeling approach applied to San Francisco Bay. PLoS ONE, 6, e27388.

United States Fish and Wildlife Service (USFWS), 2014. Bombay Hook National Widlife Refuge.

United States Geological Survey, 2012. USGS High Resolution Orthoimagry for Kent County, DE:201202 0x3000m: U.S. Geological Survey.

van Proosdij, D., Davidson-Arnott, R.G.D., Ollerhead, J., Vanproosdij, D., 2006. Controls on spatial patterns of sediment deposition across a macro-tidal salt marsh surface over single tidal cycles. Estuarine, Coastal, and Shelf Science, 69: 64–86, http://dx.doi.org/10.1016/j.ecss.2006.04.022.

Van der Wal, D., Wielemaker-Van den Dool, A. and Herman, P.M.J., 2008. Spatial patterns, rates and mechanisms of saltmarsh cycles (Westerschelde, The Netherlands). Estuarine Coastal and Shelf Science, 76(2): 357-368.

van Huissteden, J., van de Plassche, 0., 1998. Sulphate reduction as geomorphologicalagent in tidal marshes ("Great Marshes" at Barnstable, Cape Cod, USA). Earth Surface Processes Landforms, 23: 223–236.

van Proosdij, D., Davidson-Arnott, R.G.D., Ollerhead, J., 2006. Controls on spatial patterns of sediment deposition across a macro-tidal salt marsh surface over single tidal cycles. Estuarine, Coastal, and Shelf Science, 69: 64-86, doi:10.1016/j.ecss.2006.04.022.

Wallbrink, P.J., Walling, D.E., and He, Q., 2002. Radionuclide measurement using HPGe gamma spectrometry. In: (Zapata, F., ed.) Handbook for the assessment of soil erosion and sedimentation using environmental radionuclides. Kluwer Academic Publisher: 67-96.

Ward, L.G., Kearney, M.S., and Stevenson, J.C., 1998. Variations in sedimentary environments and accretionary patterns in estuarine marshes undergoing rapid submergence, Chesapeake Bay. Marine Geology, 151: 111-134.

Warren, R.S., Niering, W.A., 1993. Vegetation change on a northeast tidal marsh: interaction of sea-level rise and marsh accretion. Ecology, 74: 96–103.

Wells, J.T. and Coleman, J.M. 1987. Wetland Loss and the Subdelta Life Cycle. Estuarine, Coastal and Shelf Science, 25: 111-125.

Wetland Research Associates, Inc., 1995. Tidal wetlands characterization-then and now. Final Report submitted to the Delaware Estuary Program.

Wilson, C., Hughes, Z., Fitzgerald, D., Hopkinson, C.S., Valentine, V., and Kolker, A.S., 2014. Saltmarsh pool and tidal creek morphodynamics: Dynamic equilibrium of northern latitude saltmarshes? Geomorphology, 213: 99-115.

Wilson, K.R., Kelley, J.T., Croitoru, A., Dionne, M., Belknap, D.F., Steneck, R., 2009. Stratigraphic and ecophysical characterization of salt pools: dynamic landforms of the Webhannet salt marsh, Wells, ME, USA. Estuaries and Coasts, 32: 855–870.

Wilson, K.R., Kelley, J.T., Tanner, B., Belknap, D.F., 2010. Probing the origins and stratigraphic signature of salt pools from north-temperate marshes in Maine, USA. Journal of Coastal Research, 26(6): 1007–1026.

Young, K.E. 1985. The effect of greater snow goose, *Anser caerulescens atlantica*, grazing on a Delaware tidal marsh. M.S. Thesis, University of Delaware, Newark, DE. 63 p.

Appendix A

MARSH CORE PHYSICAL PROPERTIES DATA

Core	Interval	Loss on Ignition	Gravimetric Porosity	Dry Bulk Density (g/cm^3)
AF02A	0-2	0.18	0.77	0.56
AF02A	2-4	0.17	0.77	0.56
AF02A	4-6	0.18	0.76	0.56
AF02A	6-8	0.19	0.77	0.56
AF02A	8-10	0.20	0.78	0.52
AF02A	10-12	0.20	0.79	0.49
AF02A	12-14	0.22	0.80	0.46
AF02A	14-16	0.24	0.81	0.43
AF02A	16-18	0.22	0.82	0.42
AF02A	18-20	0.23	0.82	0.42
AF02A	20-22	0.22	0.81	0.43
AF02A	22-24	0.24	0.82	0.41
AF02A	24-26	0.26	0.83	0.39
AF02A	26-28	0.27	0.83	0.39
AF02A	28-30	0.28	0.83	0.37
AF02A	30-32	0.30	0.85	0.33
AF02A	32-34	0.32	0.85	0.33
BHIN01	0-2	0.47	0.89	0.21
BHIN01	2-4	0.47	0.88	0.23
BHIN01	4-6	0.47	0.88	0.23
BHIN01	6-8	0.48	0.88	0.24
BHIN01	8-10	0.51	0.89	0.22
BHIN01	10-12	0.48	0.90	0.20
BHIN01	12-14	0.53	0.90	0.19
BHIN01	14-16	0.44	0.90	0.19
BHIN01	16-18	0.43	0.91	0.19
BHIN01	18-20	0.44	0.90	0.21
BHIN01	20-22	0.43	0.91	0.18
BHIN01	22-24	0.49	0.91	0.17
BHIN01	24-26	0.47	0.91	0.18
BHIN01	26-28	0.52	0.90	0.18
BHIN01	28-30	0.36	0.87	0.27

BHIN01	30-32	0.38	0.90	0.21
BHIN01	32-34	0.34	0.91	0.20
BHIN01	34-36	0.33	0.91	0.19
BHIN01	36-38	0.36	0.91	0.19
BHIN01	38-40	0.35	0.91	0.19
BHIN01	40-42	0.39	0.92	0.16
BHIN01	42-44	0.34	0.92	0.17
BHIN01	44-46	0.39	0.92	0.17
BHIN01	46-48	0.47	0.93	0.14
BHIN01	48-50	0.46	0.93	0.14
BHIN01	50-53	0.44	0.91	0.18
BHIN03C	0-2	0.25	0.83	0.38
BHIN03C	2-4	0.26	0.84	0.36
BHIN03C	4-6	0.31	0.86	0.30
BHIN03C	6-8	0.45	0.89	0.21
BHIN03C	8-10	0.35	0.88	0.26
BHIN03C	10-12	0.32	0.88	0.27
BHIN03C	12-14	0.40	0.90	0.21
BHIN03C	14-16	0.44	0.91	0.18
BHIN03C	16-18	0.33	0.90	0.21
BHIN03C	18-20	0.24	0.89	0.26
BHIN03C	20-22	0.26	0.89	0.26
BHIN03C	22-24	0.26	0.88	0.27
BHIN03C	24-26	0.21	0.87	0.31
BHIN03C	26-28	0.23	0.88	0.28
BHIN03C	28-30	0.27	0.90	0.23
BHIN03C	30-32	0.29	0.91	0.19
BHIN03C	32-34	0.21	0.89	0.27
BHIN03C	34-36	0.19	0.87	0.32
BHIN03C	36-38	0.17	0.86	0.34
BHIN03C	38-40	0.18	0.86	0.33
BHIN03C	40-42	0.20	0.86	0.32
BHIN03C	42-44	0.14	0.81	0.46
BHIN03C	44-46	0.13	0.80	0.48
BHIN03C	46-48	0.15	0.81	0.45
BHIN03C	48-50	0.15	0.81	0.47
BHIN03C	50-52	0.16	0.80	0.47
BHIN03C	52-54	0.16	0.80	0.49

BHIN03C	54-56	0.13	0.77	0.57
BHIN03C	56-57	0.14	0.78	0.54
BHIS02C	0-2	0.32	0.84	0.36
BHIS02C	2-4	0.36	0.86	0.30
BHIS02C	4-6	0.36	0.85	0.31
BHIS02C	6-8	0.35	0.87	0.28
BHIS02C	8-10	0.35	0.87	0.28
BHIS02C	10-12	0.35	0.88	0.26
BHIS02C	12-14	0.34	0.87	0.27
BHIS02C	14-16	0.23	0.84	0.37
BHIS02C	16-18	0.23	0.86	0.33
BHIS02C	18-20	0.26	0.87	0.30
BHIS02C	20-22	0.25	0.86	0.32
BHIS02C	22-24	0.22	0.85	0.34
BHIS02C	24-26	0.23	0.86	0.33
BHIS02C	26-28	0.22	0.86	0.33
BHIS02C	28-30	0.25	0.88	0.28
BHIS02C	30-32	0.25	0.88	0.26
BHIS02C	32-34	0.25	0.89	0.25
BHIS02C	34-36	0.21	0.88	0.29
BHIS02C	36-38	0.16	0.84	0.38
BHIS02C	38-40	0.14	0.83	0.42
BHIS02C	40-42	0.17	0.84	0.38
BHIS02C	42-44	0.18	0.85	0.35
BHIS02C	44-46	0.17	0.86	0.34
BHIS02C	46-48	0.15	0.84	0.40
BHIS02C	48-50	0.15	0.84	0.40
BHIS02C	50-52	0.16	0.83	0.40
BHIS02C	52-54	0.15	0.82	0.43
BHIS02C	54-56	0.16	0.83	0.42
BHIS02C	56-58	0.20	0.85	0.35
BHIS02C	58-63	0.15	0.82	0.44
GI01	0-2	0.49	0.89	0.21
GI01	2-4	0.54	0.91	0.18
GI01	4-6	0.58	0.91	0.17
GI01	6-8	0.48	0.90	0.19
GI01	8-10	0.45	0.91	0.19
GI01	10-12	0.47	0.90	0.19

GI01	12-14	0.52	0.91	0.17
GI01	14-16	0.49	0.91	0.18
GI01	16-18	0.56	0.91	0.17
GI01	18-20	0.62	0.91	0.16
GI01	20-22	0.61	0.89	0.19
GI01	22-24	0.64	0.88	0.21
GI01	24-26	0.64	0.89	0.19
GI01	26-28	0.65	0.89	0.18
GI01	28-30	0.47	0.89	0.21
GI01	30-32	0.45	0.90	0.19
GI01	32-34	0.42	0.91	0.18
GI01	34-36	0.38	0.91	0.19
GI01	36-38	0.33	0.91	0.20
GI01	38-40	0.28	0.91	0.21
GI01	40-42	0.32	0.91	0.19
GI01	42-44	0.39	0.93	0.16
GI01	44-46	0.46	0.94	0.12
GI01	46-48	0.47	0.92	0.15
GI01	48-50	0.48	0.92	0.17
GI01	50-52	0.52	0.91	0.18
GI01	52-54	0.58	0.91	0.17
GI03	0-2	0.22	0.82	0.43
GI03	2-4	0.22	0.82	0.41
GI03	4-6	0.22	0.83	0.39
GI03	6-8	0.25	0.85	0.35
GI03	8-10	0.25	0.86	0.33
GI03	10-12	0.24	0.86	0.32
GI03	12-14	0.25	0.87	0.31
GI03	14-16	0.21	0.86	0.33
GI03	16-18	0.22	0.87	0.31
GI03	18-20	0.21	0.86	0.32
GI03	20-22	0.19	0.85	0.35
GI03	22-24	0.19	0.86	0.33
GI03	24-26	0.20	0.87	0.30
GI03	26-28	0.21	0.88	0.29
GI03	28-30	0.20	0.88	0.29
GI03	30-32	0.21	0.88	0.28
GI03	32-34	0.20	0.87	0.30

GI03	34-36	0.21	0.89	0.27
GI03	36-38	0.21	0.89	0.26
GI03	38-40	0.22	0.88	0.28
GI03	40-42	0.21	0.87	0.31
GI03	42-44	0.22	0.86	0.34
GI03	44-46	0.25	0.86	0.32
INT1	0-2	0.16	0.78	0.54
INT1	2-4	0.15	0.78	0.55
INT1	4-6	0.14	0.77	0.55
INT1	6-8	0.14	0.81	0.46
INT1	8-10	0.14	0.80	0.49
INT1	10-12	0.15	0.82	0.44
INT1	12-14	0.17	0.82	0.42
INT1	14-16	0.17	0.82	0.42
INT1	16-18	0.17	0.82	0.43
INT1	18-20	0.16	0.82	0.44
INT1	20-22	0.17	0.81	0.45
INT1	22-24	0.17	0.82	0.43
INT1	24-26	0.18	0.83	0.41
INT1	26-28	0.17	0.82	0.43
INT1	28-30	0.17	0.82	0.43
INT1	30-32	0.17	0.82	0.44
INT1	32-34	0.17	0.83	0.40
INT1	34-36	0.18	0.84	0.38
INT1	36-38	0.17	0.83	0.40
INT1	38-40	0.15	0.83	0.42
INT1	40-42	0.15	0.83	0.42
INT1	42-44	0.15	0.82	0.44
INT1	44-46	0.16	0.83	0.42
INT1	46-48	0.17	0.83	0.42
INT1	48-50	0.15	0.82	0.44
INT1	50-52	0.17	0.82	0.44
INT1	52-54	0.15	0.81	0.47
INT1	54-56	0.14	0.80	0.49
INT1	56-58	0.14	0.80	0.49
INT1	58-60	0.16	0.81	0.47
INT1	60-62	0.19	0.83	0.39
INT2	0-2	0.26	0.81	0.43

INT2	2-4	0.25	0.81	0.43
INT2	4-6	0.25	0.81	0.44
INT2	6-8	0.28	0.80	0.45
INT2	8-10	0.28	0.82	0.39
INT2	10-12	0.31	0.84	0.35
INT2	12-14	0.32	0.84	0.35
INT2	14-16	0.28	0.83	0.38
INT2	16-18	0.25	0.82	0.42
INT2	18-20	0.30	0.83	0.39
INT2	20-22	0.36	0.86	0.31
INT2	22-24	0.36	0.86	0.30
INT2	24-26	0.34	0.86	0.30
INT2	26-28	0.36	0.86	0.30
INT2	28-30	0.40	0.88	0.24
INT2	30-32	0.46	0.88	0.25
INT2	32-34	0.46	0.88	0.25
INT3	0-2	0.48	0.82	0.35
INT3	2-4	0.43	0.85	0.31
INT3	4-6	0.43	0.88	0.25
INT3	6-8	0.53	0.89	0.20
INT3	8-10	0.49	0.88	0.24
INT3	10-12	0.40	0.87	0.26
INT3	12-14	0.34	0.87	0.27
INT3	14-16	0.35	0.88	0.25
INT3	16-18	0.45	0.90	0.19
INT3	18-20	0.44	0.89	0.22
INT3	20-22	0.47	0.90	0.20
INT3	22-24	0.40	0.89	0.23
INT3	24-26	0.38	0.90	0.21
INT3	26-28	0.35	0.89	0.23
INT3	28-30	0.40	0.88	0.25
INT3	30-32	0.39	0.89	0.23
INT3	32-34	0.32	0.86	0.30
INT3	34-36	0.37	0.88	0.24
INT3	36-39	0.32	0.87	0.28
KELL03	0-2	0.42	0.88	0.24
KELL03	2-4	0.43	0.88	0.24
KELL03	4-6	0.50	0.88	0.23

KELL03	6-8	0.37	0.86	0.29
KELL03	8-10	0.44	0.88	0.24
KELL03	10-12	0.39	0.88	0.25
KELL03	12-14	0.33	0.88	0.26
KELL03	14-16	0.28	0.88	0.27
KELL03	16-18	0.26	0.87	0.29
KELL03	18-20	0.27	0.88	0.28
KELL03	20-22	0.29	0.85	0.34
KELL03	22-24	0.29	0.88	0.28
KELL03	24-26	0.29	0.87	0.29
KELL03	26-28	0.27	0.88	0.28
KELL03	28-30	0.30	0.89	0.24
KELL03	30-32	0.29	0.90	0.23
KELL03	32-34	0.25	0.89	0.26
KELL03	34-36	0.19	0.87	0.32
KELL03	36-38	0.17	0.84	0.38
KELL03	38-40	0.21	0.84	0.38
KENT01	0-2	0.36	0.85	0.31
KENT01	2-4	0.36	0.86	0.30
KENT01	4-6	0.38	0.86	0.30
KENT01	6-8	0.38	0.85	0.31
KENT01	8-10	0.35	0.85	0.31
KENT01	10-12	0.36	0.85	0.32
KENT01	12-14	0.37	0.86	0.30
KENT01	14-16	0.33	0.86	0.31
KENT01	16-18	0.35	0.87	0.27
KENT01	18-20	0.31	0.87	0.29
KENT01	20-22	0.34	0.86	0.30
KENT01	22-24	0.28	0.85	0.34
KENT01	24-26	0.24	0.85	0.36
KENT01	26-28	0.26	0.85	0.33
KENT01	28-30	0.25	0.85	0.35
KENT01	30-32	0.22	0.85	0.35
KENT01	32-34	0.22	0.85	0.36
KENT01	34-36	0.26	0.86	0.31
KENT01	36-38	0.30	0.87	0.29
KENT01	38-40	0.31	0.87	0.28
KENT01	40-42	0.26	0.87	0.30

KENT01	42-44	0.25	0.88	0.27
KENT01	44-46	0.24	0.89	0.26
KENT01	46-48	0.23	0.88	0.27
KENT01	48-50	0.21	0.88	0.28
KENT01	50-52	0.22	0.89	0.26
KENT01	52-54	0.21	0.88	0.29
KENT01	54-56	0.19	0.85	0.36
KENT01	56-58	0.25	0.84	0.36
KENTBS	0-2	0.39	0.83	0.36
KENTBS	2-4	0.39	0.84	0.34
KENTBS	4-6	0.48	0.87	0.25
KENTBS	6-8	0.40	0.86	0.29
KENTBS	8-10	0.37	0.87	0.27
KENTBS	10-12	0.44	0.89	0.22
KENTBS	12-14	0.41	0.87	0.26
KENTBS	14-16	0.36	0.86	0.30
KENTBS	16-18	0.34	0.87	0.28
KENTBS	18-20	0.33	0.86	0.30
KENTBS	20-22	0.36	0.88	0.25
KENTBS	22-24	0.41	0.90	0.20
KENTBS	24-26	0.35	0.90	0.22
KENTBS	26-28	0.32	0.90	0.23
KENTBS	28-30	0.30	0.89	0.24
KENTBS	30-32	0.25	0.88	0.27
KENTBS	32-34	0.30	0.89	0.23
KENTBS	34-36	0.28	0.87	0.28
KENTBS	36-38	0.27	0.87	0.30
KENTBS	38-40	0.25	0.87	0.31
KENTBS	40-42	0.23	0.86	0.32
KENTBS	42-44	0.26	0.86	0.32
KENTBS	44-46	0.19	0.81	0.45
KENTBS	46-48	0.18	0.81	0.45
KENTBS	48-50	0.19	0.81	0.45
KENTBS	50-52	0.17	0.80	0.48
KENTBS	52-54	0.17	0.81	0.46
KENTBS	54-56	0.18	0.80	0.48
KENTBS	56-58	0.21	0.80	0.47
KENTNEW	0-2	0.24	0.81	0.43

KENTNEW	2-4	0.20	0.82	0.43
KENTNEW	4-6	0.19	0.82	0.43
KENTNEW	6-8	0.21	0.83	0.40
KENTNEW	8-10	0.20	0.83	0.39
KENTNEW	10-12	0.22	0.84	0.36
KENTNEW	12-14	0.21	0.84	0.37
KENTNEW	14-16	0.17	0.83	0.42
KENTNEW	16-18	0.16	0.82	0.43
KENTNEW	18-20	0.18	0.83	0.40
KENTNEW	20-22	0.17	0.84	0.40
KENTNEW	22-24	0.16	0.83	0.40
KENTNEW	24-26	0.15	0.83	0.42
KENTNEW	26-28	0.15	0.82	0.45
KENTNEW	28-30	0.15	0.82	0.43
KENTNEW	30-32	0.15	0.82	0.43
KENTNEW	32-34	0.14	0.82	0.43
KENTNEW	34-36	0.16	0.83	0.42
KENTNEW	36-38	0.17	0.83	0.41
KENTNEW	38-40	0.18	0.84	0.39
KENTNEW	40-42	0.21	0.85	0.36
KENTNEW	42-44	0.20	0.85	0.35
KENTNEW	44-46	0.19	0.86	0.34
KENTNEW	46-48	0.16	0.84	0.37
KENTNEW	48-50	0.15	0.82	0.43
KENTNEW	50-52	0.16	0.83	0.42
KENTNEW	52-54	0.17	0.82	0.43
KENTNEW	54-56	0.19	0.83	0.40
KENTNEW	56-58	0.18	0.82	0.44
KENTNEW	58-60	0.16	0.80	0.49
KENTNEW	60-62	0.21	0.83	0.41
KENTNS	0-2	0.27	0.80	0.46
KENTNS	2-4	0.25	0.78	0.50
KENTNS	4-6	0.31	0.80	0.45
KENTNS	6-8	0.29	0.79	0.46
KENTNS	8-10	0.25	0.78	0.50
KENTNS	10-12	0.29	0.81	0.42
KENTNS	12-14	0.27	0.80	0.44
KENTNS	14-16	0.26	0.80	0.45

KENTNS	16-18	0.22	0.79	0.49
KENTNS	18-20	0.24	0.81	0.45
KENTNS	20-22	0.16	0.77	0.55
KENTNS	22-24	0.16	0.76	0.57
KENTNS	24-26	0.16	0.76	0.57
KENTNS	26-28	0.17	0.78	0.53
KENTNS	28-30	0.16	0.77	0.55
KENTNS	30-32	0.17	0.79	0.51
KENTNS	32-34	0.18	0.80	0.48
KENTNS	34-36	0.17	0.79	0.49
KENTNS	36-38	0.15	0.79	0.52
KENTNS	38-40	0.18	0.82	0.44
KENTNS	40-42	0.17	0.80	0.47
KENTNS	42-44	0.18	0.82	0.44
KENTNS	44-46	0.18	0.81	0.44
LTHB01	0-2	0.20	0.81	0.45
LTHB01	2-4	0.21	0.82	0.42
LTHB01	4-6	0.21	0.81	0.44
LTHB01	6-8	0.18	0.79	0.50
LTHB01	8-10	0.19	0.80	0.47
LTHB01	10-12	0.20	0.80	0.47
LTHB01	12-14	0.19	0.81	0.45
LTHB01	14-16	0.19	0.82	0.43
LTHB01	16-18	0.18	0.81	0.45
LTHB01	18-20	0.22	0.84	0.37
LTHB01	20-22	0.20	0.84	0.39
LTHB01	22-24	0.20	0.84	0.37
LTHB01	24-26	0.24	0.87	0.31
LTHB01	26-28	0.30	0.89	0.24
LTHB01	28-30	0.35	0.91	0.19
LTHB01	30-32	0.41	0.93	0.14
LTHB01	32-34	0.41	0.96	0.08
LTHB01	34-36	0.41	0.93	0.14
LTHB01	36-38	0.37	0.93	0.15
LTHB01	38-40	0.40	0.93	0.14
LTHB01	40-42	0.41	0.94	0.13
LTHB01	42-44	0.33	0.92	0.18
LTHB01	44-46	0.42	0.92	0.17

LTHB01	46-48	0.51	0.92	0.16
LTHB4B	0-2	0.13	0.75	0.62
LTHB4B	2-4	0.13	0.75	0.61
LTHB4B	4-6	0.14	0.77	0.56
LTHB4B	6-8	0.15	0.77	0.55
LTHB4B	8-10	0.16	0.78	0.53
LTHB4B	10-12	0.15	0.79	0.52
LTHB4B	12-14	0.14	0.77	0.56
LTHB4B	14-16	0.14	0.77	0.55
LTHB4B	16-18	0.13	0.78	0.55
LTHB4B	18-20	0.13	0.78	0.53
LTHB4B	20-22	0.13	0.75	0.61
LTHB4B	22-24	0.14	0.76	0.58
LTHB4B	24-26	0.15	0.78	0.53
LTHB4B	26-28	0.15	0.78	0.54
LTHB4B	28-30	0.14	0.77	0.56
LTHB4B	30-32	0.15	0.78	0.54
LTHB4B	32-34	0.15	0.80	0.50
LTHB4B	34-36	0.16	0.81	0.46
LTHB4B	36-38	0.16	0.82	0.44
LTHB4B	38-40	0.15	0.81	0.46
LTHB4B	40-42	0.16	0.81	0.46
LTHB4B	42-44	0.18	0.82	0.44
LTHB4B	44-46	0.16	0.83	0.42
LTHB4B	46-48	0.16	0.82	0.44
LTHB4B	48-50	0.15	0.82	0.45
LTHB4B	50-52	0.14	0.80	0.48
LTHB4B	52-54	0.15	0.80	0.48
LTHB4B	54-56	0.15	0.80	0.50
LTHB4B	56-58	0.17	0.81	0.45
LTHB4B	58-60	0.21	0.83	0.40
SD1	0-2	0.20	0.78	0.51
SD1	2-4	0.21	0.80	0.47
SD1	4-6	0.22	0.82	0.43
SD1	6-8	0.16	0.78	0.52
SD1	8-10	0.17	0.81	0.46
SD1	10-12	0.16	0.80	0.49
SD1	12-14	0.15	0.80	0.49

SD1	14-16	0.15	0.79	0.50
SD1	16-18	0.14	0.81	0.46
SD1	18-20	0.15	0.82	0.43
SD1	20-22	0.15	0.81	0.47
SD1	22-24	0.13	0.79	0.53
SD1	24-26	0.11	0.78	0.56
SD1	26-28	0.12	0.78	0.54
SD1	28-30	0.11	0.78	0.54
SD1	30-32	0.12	0.79	0.53
SD1	32-34	0.12	0.79	0.53
SD1	34-36	0.11	0.80	0.50
SD1	36-38	0.11	0.80	0.51
SD1	38-40	0.12	0.80	0.48
SD1	40-42	0.12	0.81	0.47
SD1	42-44	0.12	0.81	0.47
SD1	44-46	0.12	0.81	0.46
SD1	46-48	0.12	0.81	0.46
SD1	48-50	0.11	0.81	0.47
SD1	50-52	0.11	0.80	0.49
SD1	52-53	0.11	0.80	0.50
SD2	0-2	0.15	0.76	0.59
SD2	2-4	0.16	0.75	0.59
SD2	4-6	0.17	0.76	0.59
SD2	6-8	0.15	0.76	0.59
SD2	8-10	0.15	0.76	0.58
SD2	10-12	0.15	0.77	0.57
SD2	12-14	0.17	0.77	0.55
SD2	14-16	0.15	0.77	0.56
SD2	16-18	0.18	0.78	0.52
SD2	18-20	0.16	0.79	0.50
SD2	20-22	0.14	0.80	0.49
SD2	22-24	0.13	0.79	0.51
SD2	24-26	0.13	0.80	0.50
SD2	26-28	0.14	0.80	0.50
SD2	28-30	0.13	0.79	0.51
SD2	30-32	0.12	0.79	0.52
SD2	32-34	0.12	0.79	0.51
SD2	34-36	0.12	0.79	0.51

SD2	36-38	0.12	0.80	0.50
SD2	38-40	0.12	0.79	0.52
SD2	40-42	0.12	0.80	0.49
SD2	42-44	0.10	0.78	0.54
SD2	44-46	0.12	0.78	0.55
SD2	46-48	0.12	0.78	0.54
SD2	48-50	0.13	0.79	0.51
SD2	50-52	0.12	0.79	0.52
SD2	52-54	0.13	0.80	0.50
SD2	54-56	0.11	0.79	0.53
SD2	56-59	0.10	0.75	0.61
STEAM	0-2	0.33	0.83	0.37
STEAM	2-4	0.32	0.85	0.34
STEAM	4-6	0.28	0.84	0.37
STEAM	6-8	0.25	0.83	0.39
STEAM	8-10	0.23	0.83	0.40
STEAM	10-12	0.20	0.82	0.43
STEAM	12-14	0.19	0.82	0.43
STEAM	14-16	0.21	0.83	0.40
STEAM	16-18	0.18	0.82	0.44
STEAM	18-20	0.18	0.81	0.45
STEAM	20-22	0.16	0.79	0.51
STEAM	22-24	0.15	0.78	0.54
STEAM	24-26	0.16	0.79	0.50
STEAM	26-28	0.16	0.81	0.46
STEAM	28-30	0.15	0.81	0.47
STEAM	30-32	0.15	0.80	0.48
STEAM	32-34	0.15	0.81	0.46
STEAM	34-36	0.17	0.83	0.42
STEAM	36-38	0.18	0.82	0.43
STEAM	38-40	0.18	0.81	0.46
STEAM	40-42	0.16	0.80	0.49
STEAM	42-44	0.16	0.79	0.52
STEAM	44-46	0.16	0.80	0.48
STEAM	46-48	0.17	0.81	0.45
STEAM	48-50	0.18	0.82	0.43
STEAM	50-52	0.19	0.84	0.38
STEAM	52-54	0.22	0.85	0.35

STEAM	54-56	0.22	0.86	0.34
STEAM	56-59	0.22	0.84	0.37

Appendix B

MARSH CORE RADIONUCLIDE DATA

Core	Interval	Sample Mass (g)	Pb-210 Activity (Mbq/g)	Pb-210 Uncertainty (Mbq/g)	Bi-214 Activity (Mbq/g)	Bi-214 Uncertainty (Mbq/g)	Cs-137 Activity (Mbq/g)	Cs-137 Uncertainty (Mbq/g)
AF02A	0-2	41.30	116.44	4.18	17.02	1.22	2.82	0.61
AF02A	2-4	41.11	112.03	4.17	14.11	1.30	4.36	0.60
AF02A	4-6	43.94	99.55	3.77	15.97	1.14	4.06	0.59
AF02A	6-8	38.20	92.70	2.96	15.37	0.93	4.88	0.50
AF02A	8-10	37.37	87.42	3.83	14.49	1.23	6.07	0.70
AF02A	10-12	41.85	79.32	3.76	15.03	1.18	5.57	0.69
AF02A	12-14	41.85	72.71	3.87	13.77	1.25	6.37	0.67
AF02A	14-16	38.98	73.75	3.50	17.15	1.15	5.39	0.64
AF02A	16-18	36.82	73.01	2.66	14.19	0.89	6.15	0.52
AF02A	18-20	39.55	66.37	3.68	15.55	1.27	7.52	0.72
AF02A	20-22	35.57	66.90	3.68	13.08	1.23	8.26	0.75
AF02A	22-24	39.70	62.95	3.62	15.01	1.23	11.85	0.81
AF02A	24-26	32.44	44.03	3.29	13.23	1.17	19.55	0.87
AF02A	26-28	32.92	40.49	3.55	13.68	1.34	28.14	1.05
AF02A	28-30	39.25	39.70	2.53	15.21	0.88	26.22	0.71
AF02A	30-32	31.18	32.62	2.51	13.05	0.97	13.27	0.63

AF02A	32-34	35.50	38.45	3.09	11.52	1.19	9.59	0.75
AF02A	34-36	37.51	34.06	2.44	11.30	0.93	6.81	0.53
BHIN01	0-2	29.03	150.34	4.40	8.14	1.23	2.63	0.62
BHIN01	2-4	36.81	131.99	3.90	8.03	1.09	2.48	0.57
BHIN01	4-6	34.71	133.04	4.00	6.60	1.18	5.00	0.59
BHIN01	6-8	33.45	108.08	3.75	10.80	1.08	3.68	0.66
BHIN01	8-10	35.14	74.51	3.41	8.92	1.08	4.86	0.61
BHIN01	10-12	28.66	78.73	3.80	10.51	1.19	4.10	0.71
BHIN01	12-14	32.96	74.57	3.65	7.56	1.09	6.99	0.67
BHIN01	14-16	26.77	59.58	3.82	11.04	1.36	16.59	0.98
BHIN01	16-18	31.81	72.04	3.58	8.89	1.20	41.28	1.18
BHIN01	18-20	29.29	60.99	3.54	9.69	1.32	65.24	1.50
BHIN01	20-22	23.04	36.66	3.73	8.55	1.52	56.63	1.54
BHIN01	22-24	28.16	37.55	3.20	9.82	1.26	21.22	0.94
BHIN01	24-26	31.01	38.20	3.09	10.58	1.22	11.59	0.83
BHIN01	26-28	31.29	53.61	3.35	8.18	1.08	5.60	0.69
BHIN01	28-30	48.24	32.66	2.94	12.88	1.06	2.95	0.54
BHIN01	30-32	41.50	22.00	3.14	10.62	1.10	4.29	0.60
BHIN01	32-34	26.44	21.96	3.40	14.59	1.42	2.94	0.69
BHIN01	34-36	31.75	20.38	3.19	14.42	1.25	2.05	0.66
BHIN01	36-38	33.35	23.31	3.04	12.67	1.25	1.96	0.61
BHIN01	38-40	29.11	10.25	3.28	12.29	1.42	1.33	
BHIN01	40-42	26.19	10.64	3.35	11.89	1.38	2.30	
BHIN01	42-44	27.22	20.62	3.12	13.93	1.39	1.05	
BHIN01	44-46	23.91	11.70	3.32	12.19	1.48	2.39	
BHIN01	46-48	20.93	13.55	3.30	9.83	1.40	1.66	

BHIN01	48-50	23.32	14.80	3.14	7.13	1.39	2.48	
BHIN01	50-53	37.87	17.80	2.69	6.98	1.08	1.69	0.59
BHIN03C	0-2	34.56	121.80	4.15	12.91	1.27	2.82	0.63
BHIN03C	2-4	38.45	104.15	3.97	16.09	1.25	2.98	0.59
BHIN03C	4-6	37.65	118.98	3.94	14.95	1.15	1.98	0.59
BHIN03C	6-8	32.02	125.57	4.22	9.74	1.17	2.15	0.64
BHIN03C	8-10	37.04	96.71	3.83	13.08	1.19	3.31	0.60
BHIN03C	10-12	43.30	81.15	3.54	16.52	1.16	3.25	0.57
BHIN03C	12-14	35.22	71.41	3.58	12.40	1.22	2.83	0.60
BHIN03C	14-16	28.94	84.55	3.70	10.05	1.23	4.26	0.67
BHIN03C	16-18	32.13	76.76	3.59	13.36	1.20	6.54	0.74
BHIN03C	18-20	46.13	64.92	3.62	16.98	1.18	10.78	0.67
BHIN03C	20-22	43.62	52.83	3.25	14.60	1.08	26.05	0.84
BHIN03C	22-24	37.57	44.59	3.64	15.10	1.32	78.86	1.55
BHIN03C	24-26	38.45	45.23	3.55	16.60	1.30	50.57	1.24
BHIN03C	26-28	47.38	35.36	3.38	17.46	1.21	38.17	1.04
BHIN03C	28-30	41.30	28.78	3.24	14.79	1.21	15.43	0.75
BHIN03C	30-32	34.08	31.99	3.28	17.71	1.31	7.77	0.74
BHIN03C	32-34	39.15	31.94	3.22	19.64	1.26	6.79	0.65
BHIN03C	34-36	40.94	28.62	3.33	19.92	1.34	4.70	0.69
BHIN03C	36-38	40.58	28.52	3.46	17.97	1.35	3.98	0.63
BHIN03C	38-40	33.55	31.56	3.49	19.07	1.45	2.25	0.70
BHIN03C	40-42	37.76	23.15	3.49	20.85	1.32	2.31	
BHIN03C	42-44	39.20	25.18	3.55	21.18	1.45	1.78	
BHIS02C	0-2	24.08	150.98	7.14	15.82	1.58	2.15	
BHIS02C	2-4	32.87	173.81	6.38	15.40	1.44	1.38	0.56

BHIS02C	4-6	42.05	164.50	5.42	13.01	1.13	1.15	0.49
BHIS02C	6-8	39.09	145.43	4.65	14.72	1.00	2.30	0.43
BHIS02C	8-10	38.79	127.09	5.54	16.03	1.27	1.09	0.51
BHIS02C	10-12	35.64	124.19	5.64	14.79	1.33	1.97	0.55
BHIS02C	12-14	44.89	146.13	6.13	16.63	1.34	1.88	0.57
BHIS02C	14-16	44.55	132.42	5.98	21.12	1.41	2.79	0.53
BHIS02C	16-18	41.31	144.59	5.92	21.36	1.35	2.86	0.57
BHIS02C	18-20	46.82	115.87	4.17	19.53	0.94	3.88	0.36
BHIS02C	20-22	42.15	77.86	5.20	18.65	1.27	6.25	0.61
BHIS02C	22-24	37.57	93.83	6.31	23.76	1.61	14.82	0.96
BHIS02C	24-26	38.45	80.00	5.80	22.32	1.56	26.42	1.08
BHIS02C	26-28	47.38	80.92	5.32	18.23	1.28	29.30	1.12
BHIS02C	28-30	41.30	47.88	5.10	16.83	1.41	24.50	1.00
BHIS02C	30-32	34.08	64.48	5.64	17.82	1.52	14.12	0.92
BHIS02C	32-34	39.15	63.07	5.26	13.07	1.36	6.82	0.71
BHIS02C	34-36	40.94	58.45	5.36	20.83	1.51	6.24	0.61
BHIS02C	36-38	40.58	59.74	5.33	21.69	1.58	4.04	0.62
BHIS02C	38-40	36.56	57.44	5.41	22.97	1.63	2.01	0.67
BHIS02C	40-42	45.86	47.17	5.41	23.79	1.47	1.26	0.56
BHIS02C	42-44	40.36	62.04	5.37	21.64	1.57	1.13	0.55
BHIS02C	44-46	39.32	57.05	5.49	22.82	1.62	2.02	0.54
GI01	0-2	32.69	182.39	4.51	7.73	1.09	5.64	0.62
GI01	2-4	25.37	122.76	4.25	4.54	1.20	5.23	0.68
GI01	4-6	25.79	97.92	3.98	6.76	1.19	5.78	0.73
GI01	6-8	34.10	86.45	3.59	7.61	1.06	8.34	0.70
GI01	8-10	25.40	56.63	3.64	9.24	1.36	10.83	0.87

GI01	10-12	25.93	69.35	3.67	8.94	1.39	11.88	0.94
GI01	12-14	16.52	146.33	5.13	5.33	1.57	14.97	1.12
GI01	14-16	19.69	146.31	5.27	7.91	1.59	18.78	1.18
GI01	16-18	26.16	121.00	4.24	6.64	1.28	20.48	0.94
GI01	18-20	20.36	74.14	4.08	4.59	1.37	22.47	1.18
GI01	20-22	20.58	77.42	4.31	3.57	1.48	56.03	1.54
GI01	22-24	22.40	60.93	3.66	5.32	1.33	43.22	1.41
GI01	24-26	33.03	47.36	3.06	5.12	1.04	21.20	0.90
GI01	26-28	28.86	32.93	3.08	5.56	1.05	12.91	0.87
GI01	28-30	30.85	30.89	2.97	8.99	1.18	19.81	0.91
GI01	30-32	31.62	20.70	3.06	7.59	1.21	17.34	0.90
GI01	32-34	22.48	27.32	3.55	8.89	1.49	21.25	1.09
GI01	34-36	25.35	28.50	3.42	7.68	1.41	15.28	0.96
GI01	36-38	28.95	23.43	3.50	11.81	1.38	11.84	0.90
GI01	38-40	28.95	23.78	3.57	15.80	1.52	17.03	0.98
GI01	40-42	24.61	15.19	3.49	12.08	1.50	13.28	0.98
GI01	42-44	19.24	16.47	3.89	10.20	1.62	11.52	1.04
GI01	44-46	14.53	9.96	4.75	9.32	1.90	8.46	1.13
GI01	46-48	19.57	18.64	3.56	8.07	1.60	8.58	0.99
GI01	48-50	21.69	28.36	3.56	8.49	1.59	9.99	0.95
GI01	50-52	24.13	29.15	3.30	10.04	1.36	8.69	0.93
GI03	0-2	37.15	159.21	6.44	17.61	1.35	4.29	0.68
GI03	2-4	30.78	154.84	6.42	14.44	1.46	4.70	0.65
GI03	4-6	36.66	136.05	6.34	13.76	1.38	3.13	0.70
GI03	6-8	35.32	142.67	6.06	16.48	1.39	2.90	0.68
GI03	8-10	31.34	112.33	5.84	11.98	1.47	3.54	0.76

GI03	10-12	37.75	95.39	4.06	14.57	0.98	5.26	0.46
GI03	12-14	31.83	110.21	6.02	14.82	1.42	5.45	0.77
GI03	14-16	33.29	102.27	4.33	16.81	1.04	5.05	0.53
GI03	16-18	30.35	95.52	6.10	14.33	1.45	6.48	0.72
GI03	18-20	35.60	100.55	5.17	13.88	1.26	5.77	0.60
GI03	20-22	31.15	86.48	4.29	14.81	1.06	7.99	0.58
GI03	22-24	31.37	95.02	5.91	15.01	1.58	7.39	0.86
GI03	24-26	32.50	77.15	5.64	17.11	1.44	8.88	0.85
GI03	26-28	33.27	77.19	4.24	15.14	1.09	10.81	0.65
GI03	28-30	30.12	69.27	5.74	17.19	1.42	15.54	0.95
GI03	30-32	39.92	77.01	5.90	16.57	1.43	24.36	1.03
GI03	32-34	29.31	76.71	6.00	13.81	1.55	34.22	1.35
GI03	34-36	28.05	62.38	6.11	15.40	1.62	26.58	1.28
GI03	36-38	32.09	64.37	5.57	13.14	1.45	22.56	1.05
GI03	38-40	29.04	57.52	4.14	12.88	1.14	17.36	0.75
GI03	40-42	27.29	65.35	5.93	16.93	1.61	9.57	0.89
GI03	42-44	35.43	53.97	5.89	18.27	1.49	5.14	0.80
GI03	44-46	34.12	76.42	5.64	16.92	1.40	5.12	0.68
GI03	46-48	28.61	62.46	5.77	16.90	1.56	4.59	0.74
INT1	0-2	31.36	94.45	4.92	18.69	1.69	3.85	0.79
INT1	2-4	32.65	98.98	4.74	17.57	1.67	4.39	0.70
INT1	4-6	32.40	101.64	4.90	17.47	1.72	2.85	0.76
INT1	6-8	30.04	94.92	3.40	19.37	1.26	2.94	0.52
INT1	8-10	27.73	91.70	5.03	16.36	1.92	3.28	0.73
INT1	10-12	30.67	95.40	4.64	15.74	1.77	3.25	0.75
INT1	12-14	32.96	94.42	4.74	16.87	1.60	3.85	0.78

INT1	14-16	35.32	95.75	4.70	19.49	1.59	4.62	0.69
INT1	16-18	28.96	91.02	4.86	19.23	1.86	4.92	0.79
INT1	18-20	34.55	81.66	4.50	19.18	1.59	5.79	0.73
INT1	20-22	36.70	92.32	4.32	18.73	1.63	5.73	0.66
INT1	22-24	37.55	74.17	4.79	19.31	1.76	7.10	0.76
INT1	24-26	34.28	84.15	4.65	20.94	1.71	5.17	0.75
INT1	26-28	35.78	65.14	4.29	18.97	1.65	6.71	0.77
INT1	28-30	35.30	74.35	4.36	17.02	1.60	4.54	0.74
INT1	30-32	33.96	76.01	4.57	20.87	1.75	6.29	0.81
INT1	32-34	39.23	74.39	4.24	23.02	1.70	6.43	0.68
INT1	34-36	40.16	71.06	3.99	21.65	1.63	6.32	0.72
INT1	36-38	40.07	59.51	4.53	22.69	1.90	5.02	0.82
INT1	38-40	36.98	62.33	4.11	20.96	1.81	7.23	0.74
INT1	40-42	33.29	61.92	4.48	23.73	1.72	6.06	0.84
INT1	42-44	34.77	63.50	4.25	21.81	1.70	5.82	0.83
INT1	44-46	30.60	63.80	4.52	18.50	1.80	9.55	0.89
INT1	46-48	38.74	56.58	3.93	24.02	1.68	8.12	0.80
INT1	48-50	39.25	52.33	3.94	23.74	1.58	7.24	0.79
INT1	50-52	36.46	52.66	4.17	19.75	1.75	9.16	0.88
INT1	52-54	42.05	49.20	4.11	24.23	1.68	12.71	0.83
INT1	54-56	37.12	50.31	4.04	23.92	1.68	11.32	0.85
INT1	56-58	36.98	45.55	4.61	22.26	1.86	12.92	1.06
INT1	58-60	40.93	50.48	4.19	23.04	1.72	16.43	1.00
INT1	60-62	39.14	55.90	3.80	20.90	1.58	26.51	1.08
INT2	0-2	22.33	204.87	7.94	18.40	1.62	2.24	0.76
INT2	2-4	35.46	225.16	7.01	15.65	1.38	2.99	0.60

INT2	4-6	34.24	180.41	6.92	15.23	1.33	3.47	0.61
INT2	6-8	37.57	184.48	6.48	14.49	1.33	3.13	0.54
INT2	8-10	32.16	185.09	6.52	14.73	1.30	3.29	0.66
INT2	10-12	34.24	156.75	5.90	14.46	1.34	3.33	0.60
INT2	12-14	33.17	146.99	6.41	10.33	1.37	4.05	0.70
INT2	14-16	33.91	134.48	6.16	14.83	1.44	3.72	0.67
INT2	16-18	36.35	103.92	6.00	16.33	1.45	1.64	0.74
INT2	18-20	33.55	107.29	5.75	14.06	1.34	3.87	0.68
INT2	20-22	25.28	84.14	6.24	8.82	1.60	3.00	0.79
INT2	22-24	28.29	83.83	5.81	14.08	1.26	4.26	0.72
INT2	24-26	30.32	85.79	5.84	11.17	1.44	8.11	0.78
INT2	26-28	31.73	69.12	5.66	15.97	1.45	15.56	1.00
INT2	28-30	28.18	61.54	5.43	7.37	1.47	33.86	1.37
INT2	30-32	33.64	100.05	5.66	8.94	1.29	62.80	1.65
INT2	32-34	31.73	81.59	5.65	10.37	1.31	42.24	1.38
INT3	0-2	30.63	160.45	5.40	7.62	1.54	2.23	
INT3	2-4	35.47	172.69	5.09	10.01	1.42	0.00	
INT3	4-6	34.24	136.98	4.93	10.17	1.45	2.59	0.58
INT3	6-8	29.59	83.34	4.10	9.33	1.38	3.73	0.54
INT3	8-10	35.55	122.81	4.54	9.41	1.25	3.09	0.63
INT3	10-12	37.20	120.62	4.38	11.82	1.37	3.49	0.61
INT3	12-14	45.14	101.03	4.25	11.56	1.29	3.56	0.62
INT3	14-16	40.14	62.11	3.68	14.56	1.32	5.24	0.68
INT3	16-18	27.46	41.56	4.01	9.44	1.49	9.20	0.91
INT3	18-20	38.40	45.02	3.47	11.26	1.37	13.77	0.88
INT3	20-22	26.91	71.58	4.22	11.07	1.41	27.96	1.40

INT3	22-24	33.26	113.32	4.67	10.50	1.56	62.20	1.71
INT3	24-26	33.26	90.27	4.22	11.42	1.51	34.02	1.30
INT3	26-28	35.29	57.14	3.71	14.52	1.49	13.03	0.90
INT3	28-30	37.38	46.37	3.36	13.88	1.36	5.38	0.68
INT3	30-32	37.16	41.13	3.50	11.18	1.52	1.77	0.58
INT3	32-34	39.12	51.66	3.40	17.56	1.38	1.39	0.58
INT3	34-36	31.85	38.12	3.66	13.34	1.52	2.93	0.65
INT3	36-39	40.60	21.31	3.52	18.85	1.53	3.05	0.61
KELL03	0-2	24.12	166.83	4.71	7.76	1.36	2.52	
KELL03	2-4	27.05	126.84	4.37	7.02	1.25	2.30	0.65
KELL03	4-6	24.15	131.12	4.55	6.83	1.30	2.41	0.71
KELL03	6-8	24.81	85.50	4.24	12.70	1.49	3.02	0.79
KELL03	8-10	31.16	84.51	3.55	8.61	1.22	3.43	0.69
KELL03	10-12	29.57	65.63	3.66	9.91	1.26	6.80	0.77
KELL03	12-14	30.29	55.19	3.75	9.47	1.29	17.00	0.87
KELL03	14-16	31.84	65.17	3.78	13.38	1.24	39.53	1.21
KELL03	16-18	32.89	58.09	3.85	14.92	1.35	87.65	1.62
KELL03	18-20	27.79	72.40	3.94	12.31	1.51	40.51	1.30
KELL03	20-22	32.93	55.64	3.71	15.65	1.30	16.46	0.87
KELL03	22-24	27.98	43.40	3.64	14.39	1.46	5.09	0.78
KELL03	24-26	35.28	32.27	3.34	14.56	1.25	2.84	0.66
KELL03	26-28	34.09	26.45	3.14	16.02	1.32	2.20	0.60
KELL03	28-30	30.22	12.96	3.41	14.36	1.38	1.71	0.65
KELL03	30-32	31.41	13.16	3.21	12.96	1.30	1.99	
KELL03	32-34	31.74	14.33	3.40	14.44	1.30	1.79	
KELL03	34-36	40.36	19.68	3.11	14.47	1.27	1.51	

KELL03	36-38	34.25	16.74	3.32	0.00		1.34	
KELL03	38-40.5	34.53	18.97	3.18	14.76	1.26	1.61	
KENT01	0-2	37.17	144.38	4.26	13.40	1.19	3.76	0.61
KENT01	2-4	33.73	113.44	4.02	9.74	1.21	4.58	0.67
KENT01	4-6	36.87	96.28	3.75	10.39	1.15	3.56	0.63
KENT01	6-8	36.86	87.42	3.61	12.19	1.10	5.08	0.60
KENT01	8-10	40.22	64.60	3.39	12.50	1.13	3.29	0.60
KENT01	10-12	36.48	65.39	3.57	12.73	1.21	4.73	0.69
KENT01	12-14	41.16	69.38	3.51	12.66	1.14	5.77	0.63
KENT01	14-16	39.74	64.46	3.45	11.60	1.27	9.40	0.72
KENT01	16-18	33.94	48.32	2.65	12.14	0.93	14.38	0.62
KENT01	18-20	36.41	45.11	3.47	10.98	1.24	17.37	0.85
KENT01	20-22	36.97	46.35	3.20	12.08	1.07	45.74	1.13
KENT01	22-24	37.67	39.23	2.62	14.46	0.96	41.85	0.86
KENT01	24-26	37.15	43.13	3.35	14.08	1.27	23.30	0.95
KENT01	26-28	35.79	23.96	3.37	16.23	1.36	8.70	0.68
KENT01	28-30	37.06	29.51	3.42	17.95	1.32	3.85	0.66
KENT01	30-32	36.13	24.30	3.53	15.03	1.34	2.18	0.60
KENT01	32-34	34.71	23.41	3.37	14.41	1.40	1.83	
KENT01	34-36	34.23	24.70	2.35	14.80	0.97	0.90	
KENT01	36-38	38.41	22.61	3.09	14.77	1.27	1.34	
KENT01	38-40	38.98	16.69	3.08	15.99	1.21	0.97	
KENT01	40-42	32.91	18.17	3.05	15.38	1.23	1.38	
KENT01	42-44	38.03	20.31	2.29	14.38	0.91	0.62	
KENT01	44-46	31.36	22.19	3.37	19.43	1.42	1.32	
KENT01	46-48	30.82	19.81	3.40	16.73	1.37	0.35	

KENT01	48-50	33.15	12.64	3.44	18.02	1.38	2.07	
KENT01	50-52	35.35	21.63	3.33	14.56	1.37	0.00	
KENT01	52-54	34.19	19.16	2.43	17.52	1.02	0.00	
KENT01	54-56	32.74	17.44	3.45	20.29	1.43	2.26	
KENT01	56-58	42.34	24.69	3.11	16.72	1.19	1.16	0.55
KENTBS	0-2	32.78	167.95	4.55	10.10	1.28	1.62	0.66
KENTBS	2-4	41.63	129.70	2.82	11.26	0.80	2.68	0.39
KENTBS	4-6	32.72	126.10	3.94	7.97	1.12	2.95	0.58
KENTBS	6-8	33.76	69.97	3.80	11.03	1.24	3.05	0.63
KENTBS	8-10	38.21	68.71	3.44	12.54	1.12	3.38	0.68
KENTBS	10-12	33.32	61.03	3.38	10.18	1.10	6.20	0.73
KENTBS	12-14	33.73	86.98	3.75	10.78	1.18	11.00	0.79
KENTBS	14-16	41.22	79.84	3.69	11.07	1.20	28.38	0.97
KENTBS	16-18	40.25	54.54	3.45	11.43	1.22	67.43	1.37
KENTBS	18-20	37.34	42.33	2.67	14.86	0.97	58.14	1.01
KENTBS	20-22	42.20	48.22	3.19	13.49	1.13	16.13	0.79
KENTBS	22-24	33.29	46.93	3.32	11.07	1.30	7.40	0.69
KENTBS	24-26	33.53	40.92	3.25	12.04	1.31	3.90	0.67
KENTBS	26-28	33.21	29.42	3.28	13.05	1.31	3.42	0.64
KENTBS	28-30	32.43	22.22	3.28	12.79	1.31	2.41	
KENTBS	30-32	37.27	29.26	3.16	16.98	1.27	1.64	0.61
KENTBS	32-34	32.53	27.91	3.41	15.53	1.32	2.06	
KENTBS	34-36	34.61	28.53	3.21	15.58	1.36	2.09	
KENTBS	36-38	34.15	24.85	3.33	15.51	1.36	0.00	
KENTBS	38-40	34.93	25.54	3.20	16.30	1.24	1.48	
KENTBS	40-42	32.01	20.89	3.37	14.89	1.31	1.24	

KENTBS	44-46	40.37	25.12	3.23	20.58	1.28	1.70	
KENTBS	46-48	37.09	12.59	3.30	16.63	1.29	1.46	
KENTBS	48-50	31.08	15.76	3.71	16.69	1.53	0.00	
KENTBS	50-52	36.37	15.86	2.36	16.37	0.94	1.04	
KENTBS	52-54	39.00	17.02	3.18	18.49	1.28	0.21	
KENTBS	54-56	39.11	20.24	3.23	17.14	1.24	0.33	
KENTBS	56-58	37.64	20.50	3.22	15.23	1.29	1.47	
KENTNEW	0-2	31.32	100.87	4.14	14.04	1.30	4.26	0.66
KENTNEW	2-4	24.03	101.12	4.58	15.20	1.53	2.31	0.84
KENTNEW	4-6	26.72	102.65	4.34	14.58	1.41	2.94	
KENTNEW	6-8	34.12	95.69	3.90	14.32	1.21	3.25	0.64
KENTNEW	8-10	25.24	86.67	3.23	14.34	1.07	4.22	0.60
KENTNEW	10-12	29.00	69.27	3.65	15.03	1.28	2.54	0.68
KENTNEW	12-14	28.14	64.92	3.88	14.30	1.42	3.16	0.75
KENTNEW	14-16	29.22	70.63	2.87	13.06	1.02	4.51	0.56
KENTNEW	16-18	29.27	66.81	3.82	13.65	1.32	5.09	0.78
KENTNEW	18-20	32.10	68.15	3.70	14.94	1.32	3.27	0.73
KENTNEW	20-22	28.42	59.87	3.28	14.75	1.28	3.98	0.69
KENTNEW	22-24	33.20	56.77	2.63	13.77	0.95	6.19	0.51
KENTNEW	24-26	34.45	49.77	3.80	13.71	1.34	4.91	0.74
KENTNEW	26-28	39.19	60.10	3.60	15.32	1.24	6.28	0.71
KENTNEW	28-30	29.28	56.66	2.90	13.85	1.09	7.75	0.58
KENTNEW	30-32	33.15	52.04	3.52	16.26	1.25	7.24	0.76
KENTNEW	32-34	30.42	46.96	3.81	15.20	1.45	8.48	0.77
KENTNEW	34-36	35.03	39.35	3.64	15.83	1.35	10.12	0.77
KENTNEW	36-38	39.79	54.05	3.64	15.50	1.25	14.21	0.82

KENTNEW	38-40	39.13	52.83	3.55	14.70	1.19	16.22	0.82
KENTNEW	40-42	34.26	38.91	2.59	12.75	0.91	35.07	0.79
KENTNEW	42-44	31.90	39.95	3.59	15.51	1.31	30.32	1.06
KENTNEW	44-46	32.66	38.51	3.60	16.94	1.40	19.53	0.98
KENTNEW	46-48	30.02	31.85	3.63	13.37	1.48	17.36	0.96
KENTNEW	48-50	31.08	36.26	3.56	17.56	1.40	12.53	0.88
KENTNEW	50-52	32.17	30.33	3.71	16.43	1.43	6.19	0.76
KENTNEW	52-54	33.48	25.21	3.24	15.30	1.29	1.34	0.63
KENTNEW	54-56	37.07	33.42	3.26	14.56	1.24	2.21	0.62
KENTNEW	56-58	36.60	23.00	2.57	14.52	0.99	1.46	
KENTNEW	58-60	34.98	26.75	3.44	16.75	1.34	2.03	
KENTNS	0-2	44.82	162.36	4.79	13.13	1.45	2.02	0.57
KENTNS	2-4	42.12	141.12	3.29	13.74	1.01	2.84	0.45
KENTNS	4-6	36.71	136.18	4.65	12.36	1.37	3.86	0.65
KENTNS	6-8	31.77	85.45	4.59	13.37	1.53	1.56	0.74
KENTNS	8-10	34.30	77.52	4.36	15.43	1.56	4.54	0.64
KENTNS	10-12	35.50	76.97	4.20	14.07	1.44	2.39	0.69
KENTNS	12-14	36.44	76.21	3.22	13.96	1.14	5.06	0.54
KENTNS	14-16	38.66	74.41	3.88	17.09	1.58	6.79	0.70
KENTNS	16-18	37.06	61.22	4.01	18.69	1.54	8.58	0.81
KENTNS	18-20	41.22	54.69	2.88	18.21	1.18	35.93	0.94
KENTNS	20-22	37.63	42.96	4.10	22.52	1.58	25.14	1.13
KENTNS	22-24	37.81	43.87	3.86	22.77	1.78	10.97	0.90
KENTNS	24-26	35.57	39.28	3.45	20.89	1.48	1.43	0.61
KENTNS	26-28	33.51	35.08	2.82	19.54	1.19	1.34	
KENTNS	28-30	35.99	30.40	3.80	20.92	1.57	0.69	

KENTNS	30-32	37.25	34.58	3.77	17.36	1.64	1.69	
KENTNS	32-34	39.82	31.26	2.84	16.74	1.20	1.17	
KENTNS	34-36	35.37	32.62	3.63	19.77	1.58	1.79	
KENTNS	36-38	32.84	22.15	4.06	15.93	1.70	0.87	
KENTNS	38-40	38.82	27.94	3.80	18.03	1.63	1.26	
KENTNS	40-42	37.15	24.62	3.74	17.38	1.60	0.42	
KENTNS	42-44	35.84	27.52	3.61	16.68	1.55	0.43	
KENTNS	44-46	45.16	25.78	2.60	20.43	1.15	0.75	
LTHB01	0-2	33.33	99.21	3.63	15.45	1.23	2.70	0.61
LTHB01	2-4	40.55	81.67	3.44	16.30	1.07	2.59	0.57
LTHB01	4-6	32.18	69.39	2.70	15.99	0.95	3.55	0.48
LTHB01	6-8	36.16	63.32	3.58	13.75	1.34	3.10	0.67
LTHB01	8-10	43.44	60.40	2.55	17.20	0.85	4.27	0.44
LTHB01	10-12	39.01	62.19	3.53	17.21	1.26	4.61	0.65
LTHB01	12-14	39.52	52.41	2.61	15.02	0.89	3.75	0.48
LTHB01	14-16	38.07	47.14	3.65	15.33	1.33	5.82	0.69
LTHB01	16-18	41.44	43.98	3.44	16.08	1.26	7.37	0.65
LTHB01	18-20	40.06	46.27	3.70	15.57	1.25	11.68	0.78
LTHB01	20-22	37.89	48.58	3.39	16.88	1.19	14.43	0.82
LTHB01	22-24	42.31	44.32	2.59	15.25	0.89	25.28	0.67
LTHB01	24-26	39.93	39.44	3.49	15.73	1.26	37.90	1.09
LTHB01	26-28	40.70	43.75	3.47	15.78	1.21	34.41	1.04
LTHB01	28-30	34.66	38.82	3.50	10.40	1.14	10.45	0.77
LTHB01	30-32	24.53	38.62	3.60	9.94	1.40	3.59	0.77
LTHB01	32-34	22.40	32.96	3.57	10.10	1.43	2.36	0.75
LTHB01	34-36	25.97	24.23	2.48	8.11	1.01	2.30	0.49

LTHB01	36-38	23.09	31.46	3.43	7.58	1.49	1.45	0.76
LTHB01	38-40	22.62	18.86	3.53	11.28	1.48	1.56	0.78
LTHB01	40-42	16.60	22.07	3.04	8.89	1.40	1.08	
LTHB01	42-44	29.37	16.44	3.29	11.27	1.29	2.05	0.68
LTHB01	44-46	31.34	25.68	2.21	7.86	0.85	2.32	0.44
LTHB01	46-48	29.30	24.84	2.87	8.88	1.16	1.86	0.63
LTHB4B	0-2	32.91	108.78	4.70	20.40	1.60	3.17	0.68
LTHB4B	2-4	39.26	101.94	4.52	19.05	1.74	4.06	0.62
LTHB4B	4-6	35.15	97.68	4.49	19.05	1.76	2.12	0.63
LTHB4B	6-8	45.28	95.84	4.29	19.71	1.66	2.43	0.64
LTHB4B	8-10	40.74	95.66	3.12	19.96	1.15	2.53	0.42
LTHB4B	10-12	37.57	85.74	4.61	17.03	1.63	3.23	0.71
LTHB4B	12-14	37.82	80.36	4.13	20.00	1.50	3.00	0.69
LTHB4B	14-16	37.98	77.82	4.07	21.38	1.63	2.08	0.68
LTHB4B	16-18	35.23	71.59	3.29	20.49	1.32	3.93	0.49
LTHB4B	18-20	42.48	66.29	4.06	20.00	1.57	3.77	0.61
LTHB4B	20-22	38.68	66.98	4.17	24.23	1.64	3.51	0.65
LTHB4B	22-24	45.02	57.31	4.16	23.23	1.74	2.75	0.65
LTHB4B	24-26	40.40	63.61	4.00	22.77	1.71	3.08	0.68
LTHB4B	26-28	43.84	66.50	4.10	18.43	1.68	4.28	0.69
LTHB4B	28-30	37.07	57.89	4.21	20.92	1.65	6.30	0.69
LTHB4B	30-32	35.40	63.44	4.22	18.39	1.65	6.72	0.70
LTHB4B	32-34	36.13	53.66	4.39	18.81	1.75	7.14	0.78
LTHB4B	34-36	37.54	65.71	4.10	18.76	1.61	7.47	0.74
LTHB4B	36-38	33.78	51.36	4.30	16.76	1.76	7.29	0.82
LTHB4B	38-40	37.33	50.54	4.09	22.60	1.71	8.48	0.79

LTHB4B	40-42	32.81	51.58	4.21	20.16	1.76	14.20	1.02
LTHB4B	42-44	38.43	50.45	3.62	18.71	1.55	26.87	1.03
LTHB4B	44-46	33.49	42.22	3.45	21.22	1.37	28.48	1.07
LTHB4B	46-48	34.45	48.20	4.11	20.81	1.78	19.63	1.05
LTHB4B	48-50	38.92	36.49	4.19	20.32	1.64	17.23	0.99
LTHB4B	50-52	33.28	41.29	4.17	16.69	1.74	15.85	1.01
LTHB4B	52-54	38.58	39.19	4.12	18.25	1.65	11.70	0.86
LTHB4B	54-56	32.64	35.26	4.18	21.41	1.73	7.50	0.86
LTHB4B	56-58	36.42	39.06	2.92	19.92	1.21	4.38	0.53
LTHB4B	58-60	38.04	45.31	3.81	18.06	1.53	4.49	0.61
SD1	0-2	35.14	133.75	6.20	12.24	1.41	2.54	0.58
SD1	2-4	37.30	150.99	5.97	15.75	1.41	3.78	0.56
SD1	4-6	35.43	127.26	5.77	13.68	1.35	2.74	0.57
SD1	6-8	38.60	106.02	6.58	16.68	1.60	3.35	0.71
SD1	8-10	41.48	95.32	6.18	18.76	1.43	3.90	0.65
SD1	10-12	36.99	106.61	5.71	20.66	1.43	3.48	0.67
SD1	12-14	41.41	98.26	6.00	16.37	1.42	3.58	0.65
SD1	14-16	36.65	84.23	6.10	16.54	1.56	4.71	0.73
SD1	16-18	39.33	88.72	5.96	17.37	1.42	3.30	0.69
SD1	18-20	37.18	88.69	5.58	20.82	1.43	4.59	0.68
SD1	20-22	35.19	90.28	6.34	20.16	1.70	7.07	0.72
SD1	22-24	42.31	79.83	5.81	21.03	1.50	8.31	0.72
SD1	24-26	42.67	68.24	6.08	23.42	1.57	7.74	0.69
SD1	26-28	43.73	58.17	6.02	24.05	1.46	7.61	0.75
SD1	28-30	41.13	84.12	5.88	22.64	1.53	8.91	0.77
SD1	30-32	35.72	76.68	6.13	21.82	1.61	9.70	0.79

SD1	32-34	39.27	87.72	5.67	21.72	1.49	10.41	0.79
SD1	34-36	40.44	81.02	5.97	20.71	1.65	9.39	0.77
SD1	36-38	40.32	72.86	5.82	22.79	1.49	12.05	0.84
SD1	38-40	43.16	76.63	5.58	21.71	1.43	13.83	0.82
SD1	40-42	35.08	77.04	6.44	21.12	1.77	14.10	1.03
SD1	42-44	35.88	64.50	6.27	22.89	1.68	17.04	1.00
SD1	44-46	36.74	59.84	5.70	18.89	1.49	14.68	0.88
SD1	46-48	38.49	59.16	5.46	17.48	1.51	15.09	0.89
SD1	48-50	42.58	75.35	6.41	19.43	1.62	15.15	0.98
SD1	50-52	33.64	67.11	6.08	19.87	1.64	15.56	1.03
SD1	52-53	40.63	80.30	5.65	23.29	1.53	16.88	0.95
SD2	0-2	39.31	91.30	3.98	13.07	1.29	3.47	0.61
SD2	2-4	42.57	89.44	3.79	17.07	1.20	4.12	0.55
SD2	4-6	44.17	85.03	3.61	16.82	1.17	3.67	0.59
SD2	6-8	47.61	82.42	4.10	17.16	1.28	3.76	0.63
SD2	8-10	50.28	84.76	3.90	21.10	1.23	3.63	0.63
SD2	10-12	46.89	65.14	3.67	17.02	1.22	4.27	0.59
SD2	12-14	38.77	63.96	3.56	18.46	1.29	3.99	0.62
SD2	14-16	43.36	55.17	3.75	17.45	1.31	2.54	0.69
SD2	16-18	40.14	52.84	3.57	17.22	1.24	4.29	0.57
SD2	18-20	35.05	49.09	3.34	17.72	1.29	4.40	0.61
SD2	20-22	37.68	54.84	3.93	15.78	1.42	4.68	0.73
SD2	22-24	36.10	53.05	3.67	18.64	1.29	4.77	0.69
SD2	24-26	41.42	50.86	3.55	19.93	1.33	3.76	0.69
SD2	26-28	41.70	55.26	3.57	19.26	1.25	4.67	0.67
SD2	28-30	38.18	57.63	3.56	18.67	1.38	6.28	0.67

SD2	30-32	37.49	54.27	3.69	18.48	1.33	6.66	0.71
SD2	32-34	40.81	55.73	3.49	18.08	1.30	5.05	0.63
SD2	34-36	43.42	45.60	3.72	18.65	1.37	7.12	0.71
SD2	36-38	40.68	44.30	3.49	20.19	1.29	7.16	0.74
SD2	38-40	39.09	45.09	3.50	19.08	1.26	6.94	0.72
SD2	40-42	49.44	41.82	3.64	20.97	1.28	8.80	0.74
SD2	42-44	43.03	35.40	3.60	20.31	1.43	10.50	0.79
SD2	44-46	40.36	51.35	3.48	21.22	1.29	11.05	0.80
SD2	46-48	46.63	0.00		18.93	1.21	12.79	0.76
SD2	48-50	42.77	0.00		20.05	1.38	24.59	1.05
SD2	50-52	43.96	32.36	3.49	18.54	1.36	16.73	0.89
SD2	52-54	54.04	0.00		22.79	1.20	15.30	0.75
STEAM	0-2	32.78	188.18	4.78	15.13	1.03	4.79	0.53
STEAM	2-4	38.23	124.25	6.24	14.41	1.49	6.45	0.72
STEAM	4-6	32.23	98.04	5.82	17.57	1.38	9.99	0.81
STEAM	6-8	36.97	92.23	5.93	21.27	1.57	14.32	0.90
STEAM	8-10	33.77	90.95	4.63	20.88	1.15	20.95	0.78
STEAM	10-12	29.97	93.00	6.30	20.98	1.59	19.86	1.13
STEAM	12-14	42.40	68.58	5.74	19.14	1.53	19.50	0.94
STEAM	14-16	32.85	61.02	5.79	21.16	1.57	13.94	0.92
STEAM	16-18	32.87	62.04	5.79	19.69	1.60	8.56	0.80
STEAM	18-20	33.96	49.18	5.81	23.21	1.54	4.41	0.72
STEAM	20-22	32.95	46.32	5.39	20.94	1.55	2.02	0.67
STEAM	22-24	37.97	51.01	5.44	20.47	1.47	1.48	
STEAM	24-26	33.13	41.68	5.77	18.74	1.56	0.00	
STEAM	26-28	31.47	42.32	5.74	20.65	1.70	1.27	

STEAM	28-30	28.67	45.49	5.75	19.41	1.69	1.12	